https://doi.org/10.5194/egusphere-2025-5384
Preprint. Discussion started: 22 January 2026

Turbulence-Driven Nutrient Supply Sustains Algal Growth in the Arctic: A Modeling Approach

Giulia Castellani[1,2,3], Karley Campbell[4], Sebastien Moreau[3], and Pedro Duarte[3]

[1]University of Bremen, Institute of Environmental Physics (IUP), Bremen, Germany
[2]Deutsches Zentrum für Luft- und Raumfahrt (DLR), Institut für Physik der Atmosphäre, Oberpfaffenhofen, Germany
[3]Norwegian Polar Institute, Tromsø, Norway
[4]The Arctic University of Tromsø (UiT), Tromsø, Norway

Correspondence: Giulia Castellani (giulia.castellani@uni-bremen.de)

Abstract. Fluxes of nutrients at the ice-ocean interface are affected by the smooth or turbulent nature of the flow under the ice. The nature of the flow depends on the friction velocity, which determines the thickness of the laminar sublayer, and the roughness of the ice surface. Based on in situ boundary layer studies, the range of variability of the thickness of the laminar sublayer and that of surface roughness suggest that the flow under sea ice may easily shift from smooth to turbulent. This transition enhances nutrient exchanges at the ice-ocean interface. Despite the importance of such turbulent nutrient exchanges for sea ice algae, no current biogeochemical model accounts for the dependence of fluxes on the nature of the flow, while different approaches were previously implemented to compensate for the perceived overestimation of the nutrient limitation of ice algae growth. In the present study, we implement and test a Reynolds number-based parameterization that accounts for shifts between smooth and turbulent flow, weighing the contributions of viscosity and turbulence, in two sea-ice biogeochemical models. The results of three different case studies show that with increasing roughness, the turbulent nature of the flow contributes to larger fluxes of nutrients from the ocean to the ice. Nutrients accumulate during the winter, up to concentrations comparable to surface waters of the ocean. However, when light levels are sufficient to initiate algal growth, enhanced fluxes can support higher total production over a longer period, resulting in biomass accumulation more than twice that achieved under smooth flow conditions. In nutrient-rich waters, turbulence can supply sufficient nutrients to bring model outputs closer to observations. However, other processes, such as brine drainage in the vertically resolved model, appear to limit agreement between the two models. Our parameterization provides a more realistic representation of nutrient exchange at the sea ice–ocean interface, avoiding the need to "overtune" other model processes to reproduce observations.

1 Introduction

Sea ice in polar regions provides a unique habitat for marine algae (Tedesco et al., 2025). These ice-associated (sympagic) algae, together with phytoplankton, represent the foundation of the marine ecosystem of polar oceans that provide organic carbon to the greater foodweb. Algal phenology is constrained by the life-time of sea ice (time of ice formation and melt) and is driven by the interplay of light and nutrients as major limiting factors. The growth of ice-associated algae begins in spring with the relief of light limitation, and in the Arctic, is predominantly concentrated in the bottom most centimeters of the sea

https://doi.org/10.5194/egusphere-2025-5384
Preprint. Discussion started: 22 January 2026

ice. The availability of light to ice algae is regulated by factors such as latitude, time of year, and by ice and snow attenuation (Light et al., 2008; Castellani et al., 2022). After the onset of algal bloom, the accumulation of algal biomass is mainly limited by the amount of nutrients available since the demand of nutrients increases to support sustained growth. Thus, ultimately the availability of nutrients limits the magnitude of growth (Smith et al., 1997; Leu et al., 2015; Dalman et al., 2019). Nutrient supply to bottom-ice algae is largely sustained by interactions with the ocean beneath the ice. These processes are linked to brine dynamics and can be categorized as follows (Duarte et al., 2022; Castellani et al., 2025): 1) entrapment during sea ice growth (and release during ice melt); 2) flushing from the surface, active only during summer surface melting and rain events; 3) brine gravity drainage, driven by density instability of the brine; 4) molecular diffusion; and 5) turbulent diffusion, driven by friction velocity at the ice-ocean interface (e.g., Cota and Horne, 1989; Cota and Sullivan, 1990; Duarte et al., 2017; Mortenson et al., 2017). The ability of biogeochemical models to properly represent algal phenology thus relies to a great extent on their capacity to simulate both light transmission through snow-covered sea ice, and the exchange of nutrients at the ice-ocean interface.

Existing sea-ice biogeochemical models apply different approaches to compute nutrient fluxes between the ocean and the ice bottom (Castellani et al., 2025). Most models treat such exchanges as a diffusive process (Arrigo et al., 1993, 1997; Jin et al., 2006, 2012; Nishi and Tabeta, 2005; Deal et al., 2011; Pogson et al., 2011; Elliott et al., 2012; Mortenson et al., 2017, 2018; Hayashida et al., 2019). Only few models account for the entrapment/release during ice growth/melt (Vancoppenolle et al., 2010; Tedesco et al., 2010; Tedesco and Vichi, 2014; Watanabe et al., 2015) and even fewer models account for the contribution of turbulence (Sibert et al., 2010; Haddon et al., 2024). Recently, driven by the perception that nutrient limitation may be overestimated in some models, Duarte et al. (2022) included turbulence-driven nutrient exchanges in the Jeffery et al. (2011) model. Their results indicate that, when light limitation is relieved simulated algal growth increases substantially due to the alleviation of nutrient limitation under turbulent conditions. These findings support our argument that the characteristics of under-ice flow should be explicitly considered when describing fluxes at the ice–ocean interface.

The physical representation of flow beneath sea ice grounded in the ocean boundary layer studies of McPhee (1979, 1982, 1983). Based on under-ice measurements, Shirasawa and Grant Ingram (1991) showed that the flow can be hydraulically smooth (so of viscous nature), or hydraulically rough (of turbulent nature), or in transition between the two regimes. Eddy-covariance studies (Long et al., 2012) confirmed that the under-ice environment may be dominated by viscosity or turbulence. The shift between viscosity- and turbulence-dominated regimes under sea ice results from an interplay between current velocity and sea ice bottom roughness (Shirasawa and Ingram, 1991). The roughness Reynolds number (Re^*), which measures the ratio between inertial and viscous forces, may thus be used to evaluate the type of regime dominating the flow (Olsen et al., 2019, and references therein).

The main goal of this study was to implement and test a formulation to compute nutrient exchanges at the ice-ocean interface that weighs the contribution of viscosity and that of turbulence based on shear velocity and sea ice roughness. The formulation is applied to two sea-ice biogeochemical models: the Los Alamos sea ice model CICE + Icepack (Hunke et al., 2015) and the Sea Ice Model for Bottom algae SIMBA (Castellani et al., 2017). This provides experimental evidence to the conclusions presented in Duarte et al. (2022) by evaluating the effect of this parameterization in three case studies covering diverse sea-ice

https://doi.org/10.5194/egusphere-2025-5384
Preprint. Discussion started: 22 January 2026

regimes. Section 2 presents the parameterization developed and the models used. Section 3 outlines the main results that are then discussed in Section 4. Finally, a summary and conclusion are provided in Section 5.

2 Methodology

2.1 Parameterizing the role of turbulence on nutrients exchange

The oceanic boundary layer under sea ice is conceptually divided into a thin molecular or viscous sublayer in which viscous effects dominate, a transition region influenced by both viscous and turbulent flow, and a fully turbulent region in which the ocean current is well represented by a logarithmic law known as the "law of the wall" (Shirasawa and Ingram, 1991). The thickness and structure of these different layers is affected by the velocity profile and by the roughness of the surface, as was shown by previous studies for the case of general surfaces (e.g., Kadivar et al., 2021) and for the particular case of sea ice (McPhee, 2008). Surface roughness increases flow instability near the wall, which can lead to increased localized turbulence disrupting the viscous sublayer. This concept was described in Nikuradse (1933) where the author experimentally quantified how roughness determines a shift from the smooth flow regime to the turbulent one. In the smooth regime, the viscous sublayer is still intact and the exchange processes at the ice-ocean interface can be well described by molecular diffusion in a scheme similar to that of Lavoie et al. (2005):

$$F_{\text{Mol}} = -K_D \frac{C_w - C_i}{\delta Z} \tag{1}$$

where K_D is the molecular diffusion coefficient taken as in Mann and Lazier (2005) equal to 10^{-9} m^2 s^{-1}, $C_{w,i}$ are the nutrient concentrations in the ocean and at the ice-ocean interface, respectively, and δZ is the thickness of the molecular sublayer. In the turbulent regime, however, the molecular sublayer may be destroyed by the interaction between the flow and the roughness elements, and thus the exchange process can be described by turbulent exchange as presented in Duarte et al. (2022), following (McPhee, 2008):

$$F_{\text{Turb}} = -\alpha_s \cdot u^* \left(C_w - C_i\right) \tag{2}$$

where u^* is the friction velocity (m s^{-1}), and α_s is an interface salt–nutrient exchange coefficient (dimensionless) set at 0.6 $\times$ 10^{-3} in CICE + Icepack (McPhee, 2008). In SIMBAv2.0 we had to lower the value of α_s due to possible instabilities so we set the value to 0.6 $\times$ 10^{-4}. For computing the friction velocities we use a drag coefficient of $C_d^w = 0.536 \times 10^{-3}$ in both models following the standard approach of CICE + Icepack (Hunke et al., 2015)

We developed a conceptual model that takes into account the different flow regimes i.e., smooth or turbulent, that can occur at the bottom of the ice, as well as the transition between the two (Figure 1). The total flux F_T is then a weighted contribution of the two regimes:

https://doi.org/10.5194/egusphere-2025-5384
Preprint. Discussion started: 22 January 2026

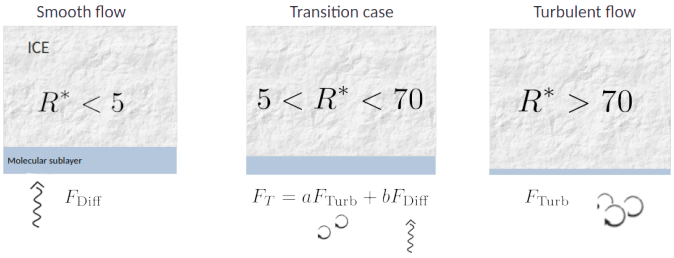

Figure 1. Soncpetual representation fo the parameterization developed which accounts for the nature of the flow under the ice (smooth vs turbulent) by weighting the contribution of molecular diffusivity or turbulent exchange through the Reynolds number R^* in computing the fluxes at the ocean-ice interface.

$$F_T = aF_{\mathrm{Diff}} + bF_{\mathrm{Turb}} \tag{3}$$

The two weights a and b are defined so that $a = 1$ and $b = 0$ in the full smooth regimes, and vice versa in the full turbulent regime. Between these two regimes, a and b decrease/increase linearly between 0 and 1. In order to define a and b, we use the roughness Reynolds number (Shirasawa and Ingram, 1991) Re^*:

$$Re^* = \frac{h_s u^*}{\nu} \tag{4}$$

where h_s is the mean height of the surface protrusions and ν is the kinematic viscosity ($\nu = 2.1 \times 10^{-6}$ m^2 s^{-1}). Note that h_s relates to the surface roughness parameter z_0 through the relation $h_s = 30z_0$. Previous studies (Nikuradse, 1933; Shirasawa and Ingram, 1991) showed that the flow is hydraulically smooth for $Re^* < 5$ and hydraulically rough for $Re^* > 70$. In the case $5 < Re^* < 70$ the flow is in transition and is influenced by both viscosity and turbulence and the total flux of nutrients is given by equation (3).

The mean height of the surface protrusions h_s needs to be prescribed. The literature values vary between less than a mm to a few centimeters. Here, based on measurements by McPhee (2002) and McPhee (2008) we used values between a minimum of $h_s = 0.6 \times 10^{-3}$ m in the case of very smooth ice surface, and a maximum of $h_s = 0.18$ m, for a rough bottom surface. As described in Section 3 such values encompass the different flow regimes from smooth to fully turbulent.

2.2 Model description

We implemented and tested the Reynolds number parameterization in the Los Alamos (CICE + Icepack) (https://https://bb.cgd.ucar.edu/cesm/forums/cice-consortium.146/, last access: 23 January 2025) (e.g. Hunke et al., 2015; Jeffery et al., 2016) and in the new version of the SIMBA (Castellani et al., 2017) sea ice models. The former includes a vertically resolved biogeochemical setup, whereas the latter is based on bottom ice biogeochemistry.

https://doi.org/10.5194/egusphere-2025-5384
Preprint. Discussion started: 22 January 2026

2.2.1 CICE + Icepack

The Los Alamos Sea Ice Model includes two independent packages: CICE, for computing ice dynamic processes, and Icepack, that computes ice column physics and biogeochemistry. The model set-up used in the present study is described in Duarte (2025a) and Duarte (2025b) and available at the git repositories (https://github.com/pduarte8/CICE, last access: 28 October 2025, and https://github.com/pduarte8/Icepack, last access: 18 October 2025). As explained in Duarte et al. (2022), both CICE + Icepack are used together by defining a 1D vertically resolved model with 1 snow layer and 15 ice layers and 5 x 5 horizontal cells. Therefore, ice column physics and biogeochemistry are calculated by Icepack, but CICE is the model driver. The input file is the same as the one used in Duarte et al. (2022) and we refer to their Tables S1 and S2 for a list of the parameters used.

We implemented equations (2) - (4) in Icepack file icepack_ brine.F90, in the subroutine compute_microS_mushy. This implied adding a parameter (h_ iceruf, h_s in equation (4)) to the file icepack_ parameters.F90.

2.2.2 SIMBA

We use a new version of the SIMBA model (Sea Ice Model for Bottom Algae) that was further developed from its first application in Castellani et al. (2017) and has a Git repository (https://github.com/EyringMLClimateGroup/Castellani2025_GMD_SIMBA2, last access: 21 October 2021) under Castellani (2025). Version 2 of SIMBA includes two more limiting nutrients: silicate and phosphate, besides the original nitrate. Another further development is the transition from a fixed cell stoichiometry to a variable Chla:C ratio as a function of nutrients concentration and light availability. This choice is particularly relevant for sea ice, where algae experience wide fluctuations of irradiance, in order to enhance the realism of the model (Ayata et al., 2013). In SIMBAv2.0, nutrients are exchanged at the sea-ice–ocean interface during ice growth and melt, flushing, through molecular diffusion, turbulence, and by the combination of processes described in equation 3. In the way it is coded, SIMBAv2.0 allows high flexibility; indeed, through several flags, it is possible to switch on and off the different terms for the resupply of nutrients. Similarly, the use of flags allows to select the limiting nutrient(s). The model equations and parameters used are presented in Appendix A.

SIMBAv2.0 is only a biogeochemical module so it needs the physics to be prescribed as forcing. In this study, we use the results for ice thickness from CICE + Icepack as input for SIMBAv2.0 for all three case studies. Moreover, SIMBAv2.0 resolves only biogeochemical processes at the bottom of the ice. The thickness of the bottom layer can be chosen according to the resolution of the data used for comparison - in the present study we set it to 10 cm for MOSAiC and N-ICE2015, and to 3 cm for Resolute (see also Section 2.4).

2.3 Forcing data

We apply the new parameterization of nutrient exchanges at the ice–ocean interface to both models and test them in three contrasting case studies — two from the Nansen Basin (Arctic Ocean), based on forcing data and ice floes monitored during the N-ICE2015 (Granskog et al., 2019), and the MOSAiC (Nicolaus et al., 2012; Shupe et al., 2022; Rabe et al., 2022) expeditions, and one from Resolute Bay in the Canadian Arctic (Mortenson et al., 2017). Data from the N-ICE2015 expedition and from

https://doi.org/10.5194/egusphere-2025-5384
Preprint. Discussion started: 22 January 2026

Table 1. Summary of simulations for the different case studies.

case study	ice type	location	start	end	h_s values used (m)
MOSAiC	FYI	Nansen Basin	24 November 2019	26 July 2020	0.6 10^{-3}, 0.0025, 0.005, 0.01, 0.18
MOSAiC	SYI	"	"	"	"
N-ICE2015	refrozen lead	"	24 April 2015	6 June 2015	"
Resolute	landfast FYI	Canadian Arctic	1 February 2010	18 June 2010	"

Resolute Bay were detailed in previous studies (Duarte et al., 2017, 2022; Mortenson et al., 2017). Therefore, here we briefly detail only the MOSAIC data.

The Multidisciplinary Drifting Observatory for the Study of Arctic Climate (MOSAiC) expedition took place from October 2019 to July 2020 with the aim of measuring a multitude of variables at a variety of spatial scales in the coupled atmosphere-ice-ocean system along the transpolar drift throughout a whole annual cycle. Expedition and data sampling are largely described in Shupe et al. (2022), Nicolaus et al. (2022), Rabe et al. (2022), and Fong et al. (2024), so we defer the reader to those references for a detailed description. The observational data collected during MOSAiC and used in this study to force the models are described in detail in Gu et al. (2024), here we will only provide a summary (see also Figure 2). The atmospheric variables include: 6-hourly surface downward shortwave and longwave radiation, daily 2 m air temperature and specific humidity, and 10 m wind speed. The oceanic data consist of daily 10 m sea temperature and salinity averaged from 8 CTD buoys, and 3 m sea temperature, salinity, and current velocity averaged from 4 autonomous ocean flux buoys. Following Gu et al. (2024) we prescribe snow depth. Observations of snow depth and ice thickness were obtained from the snow and ice mass balance buoy-array, particularly the T63 buoy (Lei et al., 2022) that was located on a second year ice (SYI) floe. We force the biogeochemistry module of CICE + Icepack and SIMBAv2.0 with observed nutrient concentrations of surface water (Torres-Valdés et al., 2024a, b, and figure 2e). Initial conditions for sea ice physical and biogeochemical variables are from ice coring data collected on November 25th, 2019 (Oggier et al., 2024a, b). Observations of sea ice draft from ice cores are shown in Figure 2c, however from the data we omitted a measurement taken at the end of March right after a rafting event (Angelopoulos et al., 2022), since with CICE + Icepack in the configuration used in the present study we can only simulate thermodynamic growth.

2.4 Model simulations

We compare the results of the runs performed with the new parameterization in which we vary the height of the surface roughness protrusions h_s. The minimum value used is h_s = 0.6 10^{-3} m, which corresponds to a fully molecular regime, and a maximum of h_s = 0.18 m, which corresponds to a fully turbulent regime (Section 3). The values in between are 0.0025, 0.005, and 0.01 m. In the MOSAiC case we perform simulations for both first-year ice (FYI) and second-year ice (SYI), but we present and discuss results for only FYI, except when specified otherwise. Table 1 list the simulations performed and the main characteristics for each case study.

https://doi.org/10.5194/egusphere-2025-5384
Preprint. Discussion started: 22 January 2026

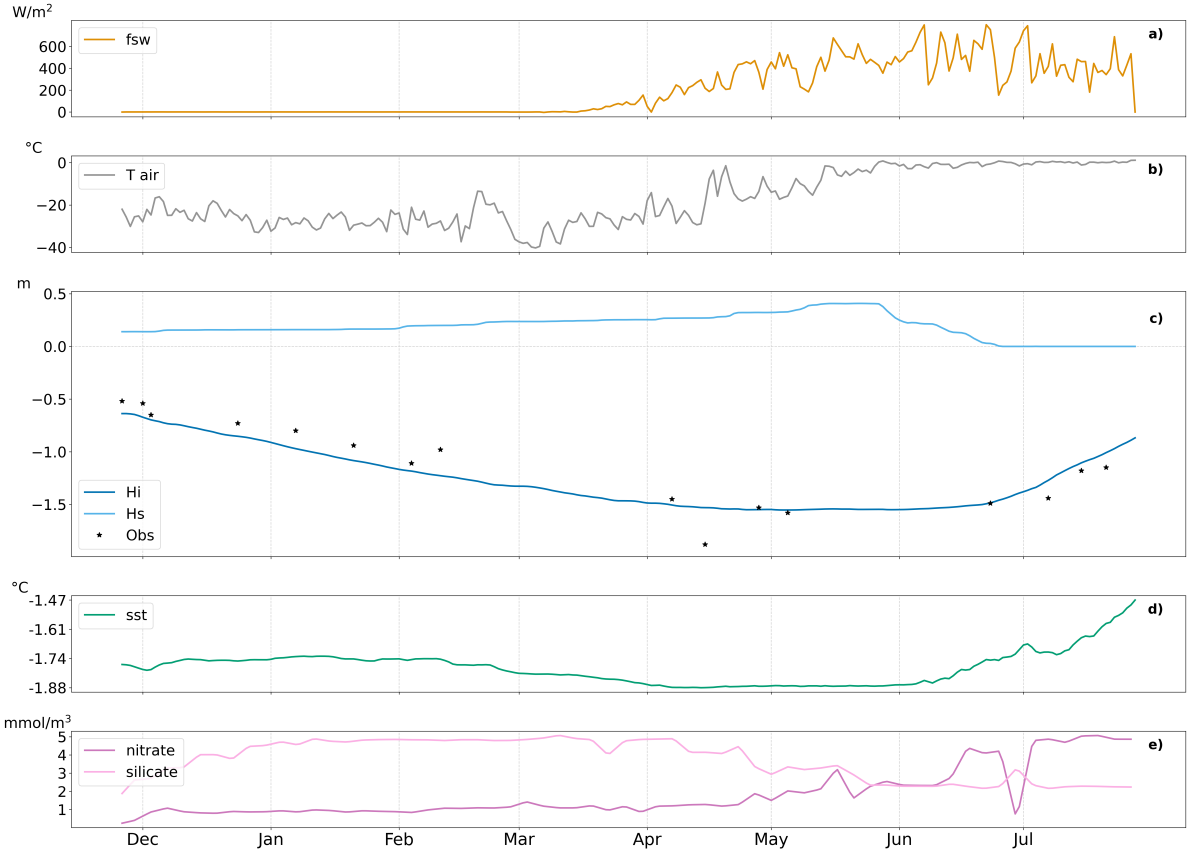

Figure 2. Overview of the forcing for the MOSAiC study case. Atmospheric forcing: a) downward shortwave radiation, and b) 2 m atmospheric temperature; oceanic forcing: d) sea surface temperature, and e) nutrients concentration in the water. Panel c) shows snow depth that is prescribed in both CICE + Icepack and ice thickness as simulated by CICE + Icepack and used to force SIMBAv2.0. Starts in panel b) represents observations collected during the coring events at the FYI site.

3 Results

3.1 MOSAiC case study

The friction velocity u^* ranged between nearly zero and 0.02 m s^{-1} (Figure 3a). Although the Reynolds number Re^* correlated with u^*, its magnitude was largely dependent on h_s (Figure 3b). With $0.0025 \leq h_s \leq 0.01$ m, Re^* remained between 5 and 70, implying that the flow regime was in transition between smooth (viscosity-dominated) and turbulent. Therefore, both molecular diffusion and turbulence contributed to the nutrient fluxes. In the case of the lowest h_s (= 0.6×10^{-3} m), Re^* was always < 5, implying that the flow was smooth and nutrient exchanges were driven only by molecular diffusion. For the largest h_s values (= 0.18 m), the Reynolds number was always above 70, so the fluxes were entirely driven by turbulence (c.f. 2.1).

https://doi.org/10.5194/egusphere-2025-5384
Preprint. Discussion started: 22 January 2026

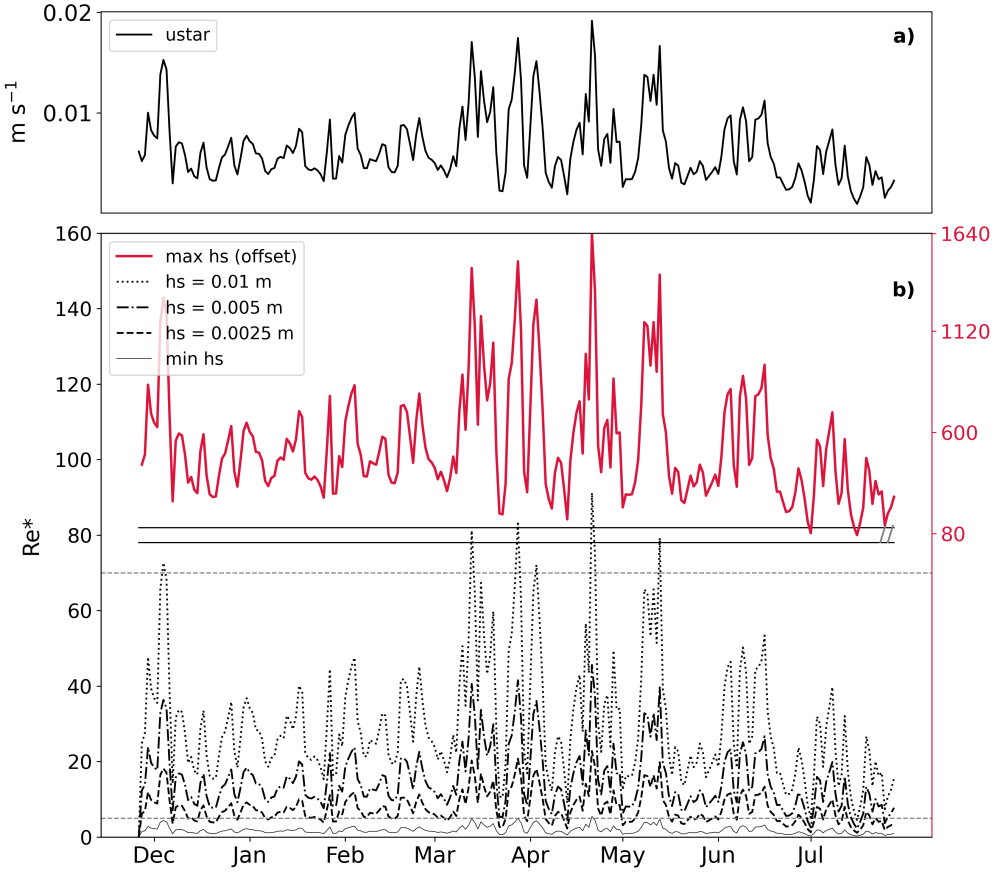

Figure 3. MOSAiC case study: a) Friction velocity; b) roughness Reynolds number Re^* for the all the different size of roughness elements tested. The horizontal dashed lines at Re^*= 5 and Re^*= 70 depict the upper limit for a smooth flow and the lower limit for a rough turbulent flow, respectively. Note that the values of Re^* for the maximum roughness (red colour) are represented on a different scale (y-axis on the right side).

https://doi.org/10.5194/egusphere-2025-5384
Preprint. Discussion started: 22 January 2026

Our analysis will focus on nitrate, the primary nitrogen source for the spring bloom (see below), and silicic acid (reported in the Supplementary Material) to compare nutrient concentrations and fluxes across different simulations. The fluxes of nitrate at the ice-ocean interface were predominantly negative (from the ocean to the ice) using either CICE + Icepack or SIMBAv2.0 (Figures 4a, 5a respectively). However, their magnitude was larger in the former model. The larger negative values occurred in spring-summer, precisely in June (in the case of CICE + Icepack) and May (SIMBAv2.0). The variability of fluxes preceding the spring period (before May) was relatively low. Fluxes increased with h_s in both models, but more notably in CICE + Icepack. Here, fluxes were very close to zero in the case of very smooth ice, but increased to -1.25 $\times$ 10^{-6} mmol m^{-2} s^{-1} when the roughness increased to the maximum value tested. At the beginning of the simulation period (Nov-Dec) the large gradient of nitrate between the sea ice bottom and the ocean caused fluxes in SIMBAv2.0 as large as 3.5 $\times 10^{-7}$ mmol m^{-2} s^{-1}. Silica fluxes are presented in the supplementary material (Figure S1).

Both models showed an initial increase in nitrate concentration at the ice bottom (Figures 4b and 5b). We note here that CICE-Icepack resolves biogeochemistry in 15 layers within the ice column. Thus, in order to select the bottom 10 cm we apply a weighted average of the number and portion of layers that are included in this depth range. In CICE + Icepack concentrations stabilize around 0.5 mmol m^{-3} and show no trend during winter. A maximum is reached in mid-June, right after the maximum of ocean-ice fluxes. In SIMBAv2.0 the concentration of nitrate stabilizes at values between 0.1 (minimum h_s) and 1.0 mmol m^{-3} ($h_s \geq 0.05$) depending on ice roughness, and show no or very little increase until mid February. Similarly to CICE + Icepack, the maximum concentration is reached after the maximum in ocean-ice fluxes, but earlier in the season (mid-May). In both models, the bottom of the ice becomes depleted in nitrate right after reaching a maximum concentration. The depletion of nitrate corresponds with the co-occurring ice algal blooms (Figures 4c and 5c). Ice algal biomass is presented as chlorophyll *a* (chl *a*) concentration. In CICE + Icepack biomass is calculated in nitrate units, so we follow Duarte et al. (2017) and apply a conversion factor of 2.1 mg chl *a* mmol N^{-1} (Smith et al., 1993). Differently, SIMBAv2.0 has a variable Chla:C, and thus Chla:N, ratios so chl *a* content is computed at each time step. The time series of Chla:C is shown in the supplementary material. Chl *a* remains close to zero until spring and reaches its maximum in June in both models. While predicted nitrate concentrations at the ice bottom were comparable for both models, SIMBAv2.0 predicted larger ice algal biomass with a maximum about twice that in CICE + Icepack. Compared with observations, CICE + Icepack exhibits bottom nutrient values lower than those measured (Figure 4b), whereas SIMBAv2.0 shows larger values (Figure 5b). Both models, however, fail to capture the full variability observed, which may partly reflect spatial heterogeneity in the ice core data.

The patterns described above were the same for all tested h_s, except the smallest value, when exchanges were entirely dominated by molecular diffusion. In CICE + Icepack, when the ice is smooth (min h_s) nitrate concentration starts to decrease already in April with the bottom of the ice becoming completely nitrate-depleted at the end of May, thus preventing any significant algal growth. SIMBAv2.0 exhibits a similar pattern, with nitrate concentrations being lower under very smooth ice, strongly limiting algal growth.

In CICE-Icepack the concentration of nitrate is larger at the bottom rather than in the ice interior (Figure 6, lower row), this is true for all values of h_s. In the case of smooth ice, the decrease in nutrient concentration seen at the end of April in the sea ice bottom (Figure 4b) extends up to 50 cm in the ice column. For rougher ice, the largest concentration of nutrients is

https://doi.org/10.5194/egusphere-2025-5384
Preprint. Discussion started: 22 January 2026

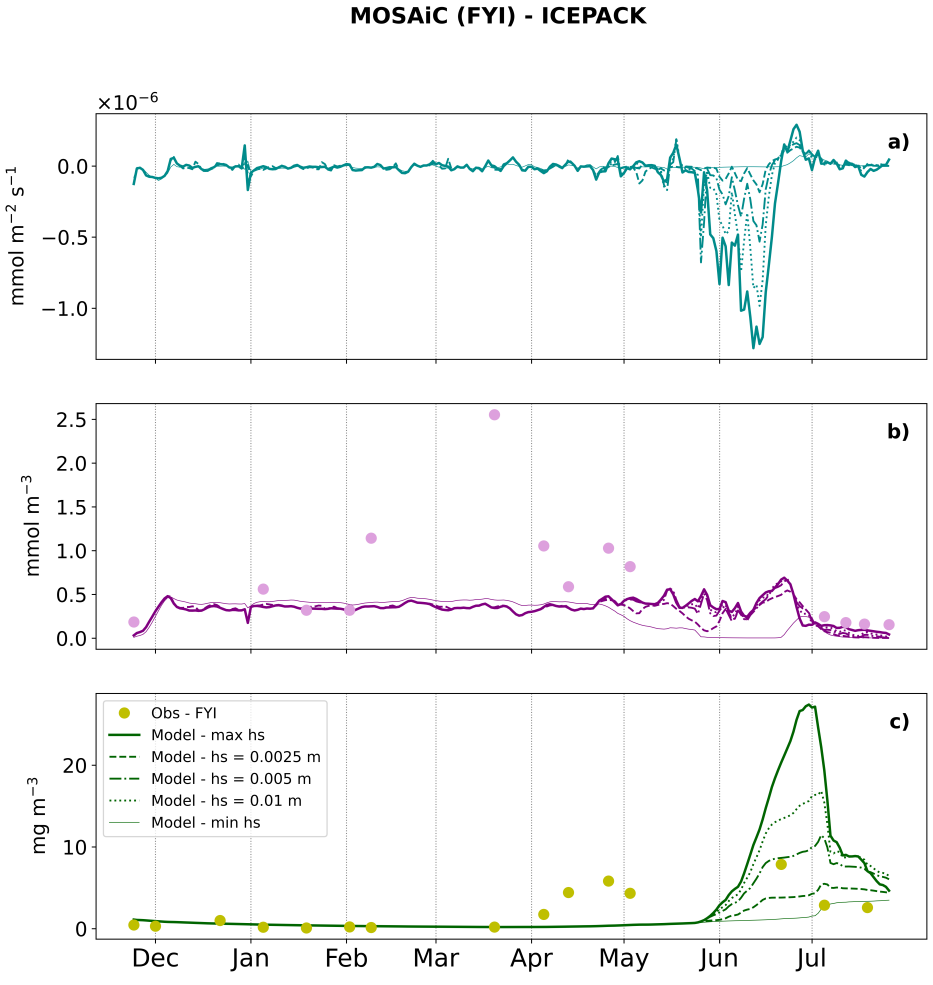

Figure 4. MOSAiC case study: CICE + Icepack results for all tested sea ice roughness values: a) Nitrate fluxes at the ice-ocean interface; b), c) Nitrate and chl *a* concentration at the sea ice bottom 10 cm, respectively. Dots represent observations from ice cores collected on FYI.

https://doi.org/10.5194/egusphere-2025-5384
Preprint. Discussion started: 22 January 2026

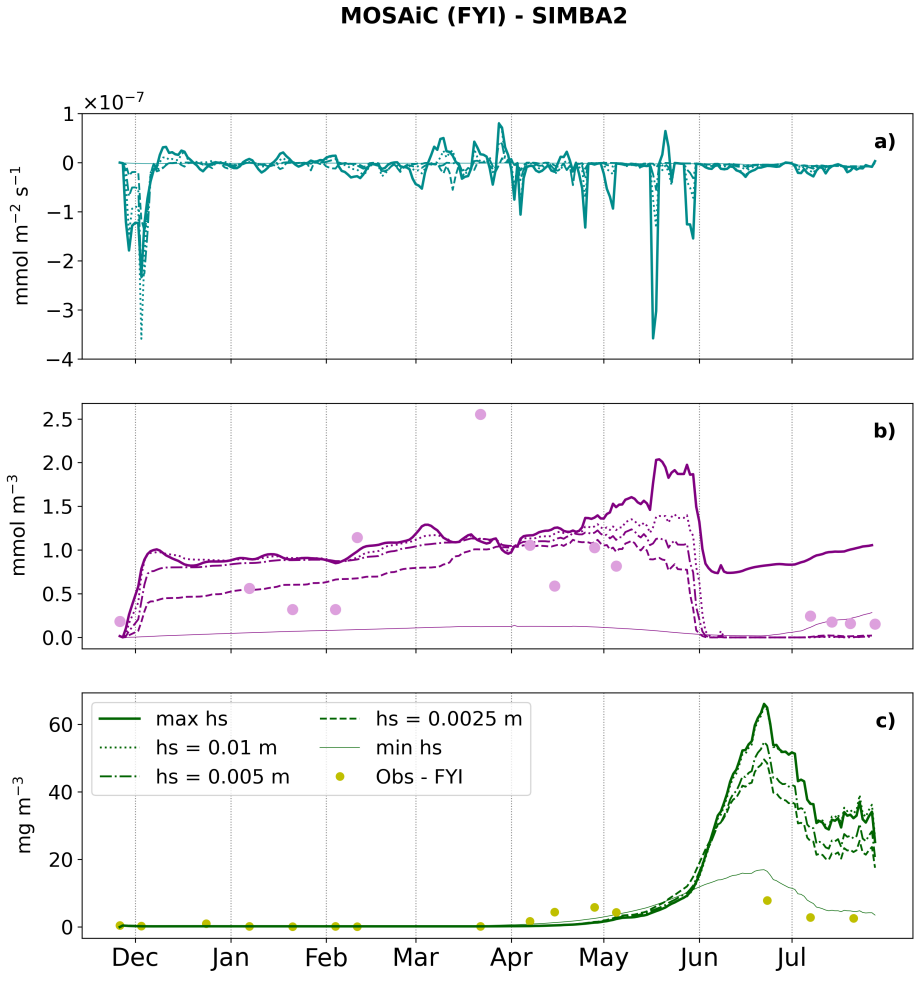

Figure 5. Same as Figure 4 but for SIMBAv2.0 results.

https://doi.org/10.5194/egusphere-2025-5384
Preprint. Discussion started: 22 January 2026

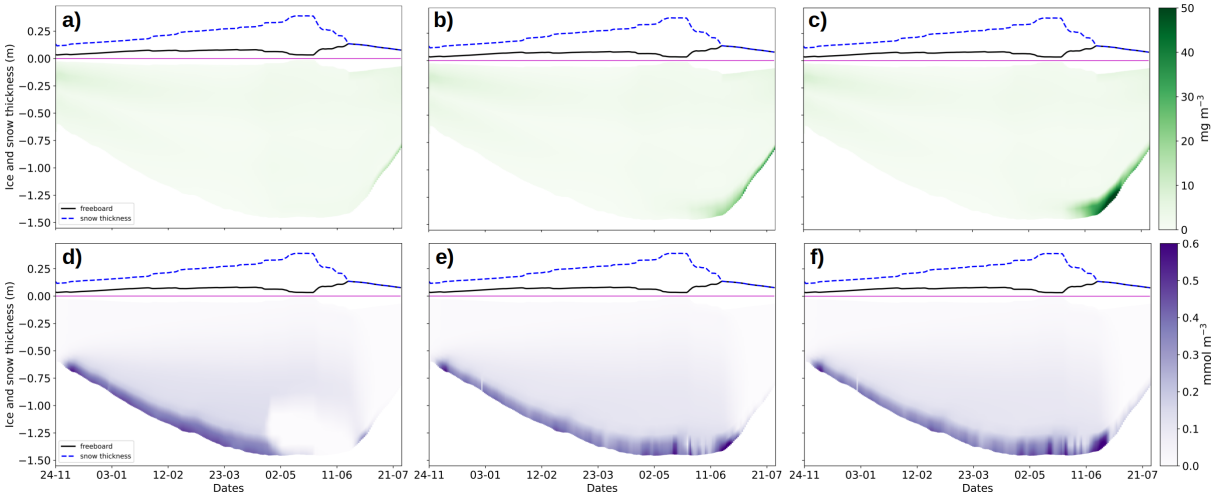

Figure 6. MOSAiC case study: Vertically resolved chl *a* and nitrate concentration (top row and lower row, respectively) in CICE + Icepack in the case of a-d) minimum h_s; b-e) h_s = 0.005 m; c-f) maximum h_s. The blue dashed and the black lines represent snow height and freeboard, relative to the sea level (magenta line).

visible in mid June in the bottom 25 cm of sea ice, mirroring what is seen already in the bottom 10 cm. Algae remain mostly concentrated at the ice bottom in all simulated cases.

3.2 N-ICE2015 case study

The results presented here are from a refrozen lead detailed in previous studies and reaching a maximum ice and snow thick-
210 nesses of 30 cm and a few millimeters, respectively (Duarte et al., 2017, 2022). The refrozen lead was monitored regularly between its formation on the 24th of April until the beginning of June 2015. Friction velocities were in the same range of the MOSAiC case (0.0 - 0.02 m s^{-1}), but with fewer values exceeding 0.01 m s^{-1} (Figure 7a). Also in this case the flow was smooth under the smallest h_s, while for maximum roughness the flow was fully turbulent. For the values in between, the flow was in transition (Figure 7b). Algal biomass followed the same pattern observed in the MOSAiC case for both models:
215 greater sea-ice roughness led to increased algal growth (Figure 8). Also in the N-ICE2015 case, SIMBAv2.0 accumulates more algal biomass than CICE + Icepack. Both models showed improved agreement with observations compared to the earlier case. It should be noted, however, that CICE + Icepack was previously tuned using this dataset (Duarte et al., 2017) on this data set, and SIMBAv2.0 uses the same parameters as CICE + Icepack to ensure comparability; therefore, it is not surprising that SIMBAv2.0 also reproduces observations more accurately in the N-ICE2015 case.

220 ### 3.3 Resolute case study

Friction velocity remained always below 0.01 m s^{-1} during the Resolute time series (Figure 9a). For most of the roughness values above the minimum, however, the flow remains in transition between smooth and turbulent, despite the low Reynolds

https://doi.org/10.5194/egusphere-2025-5384
Preprint. Discussion started: 22 January 2026

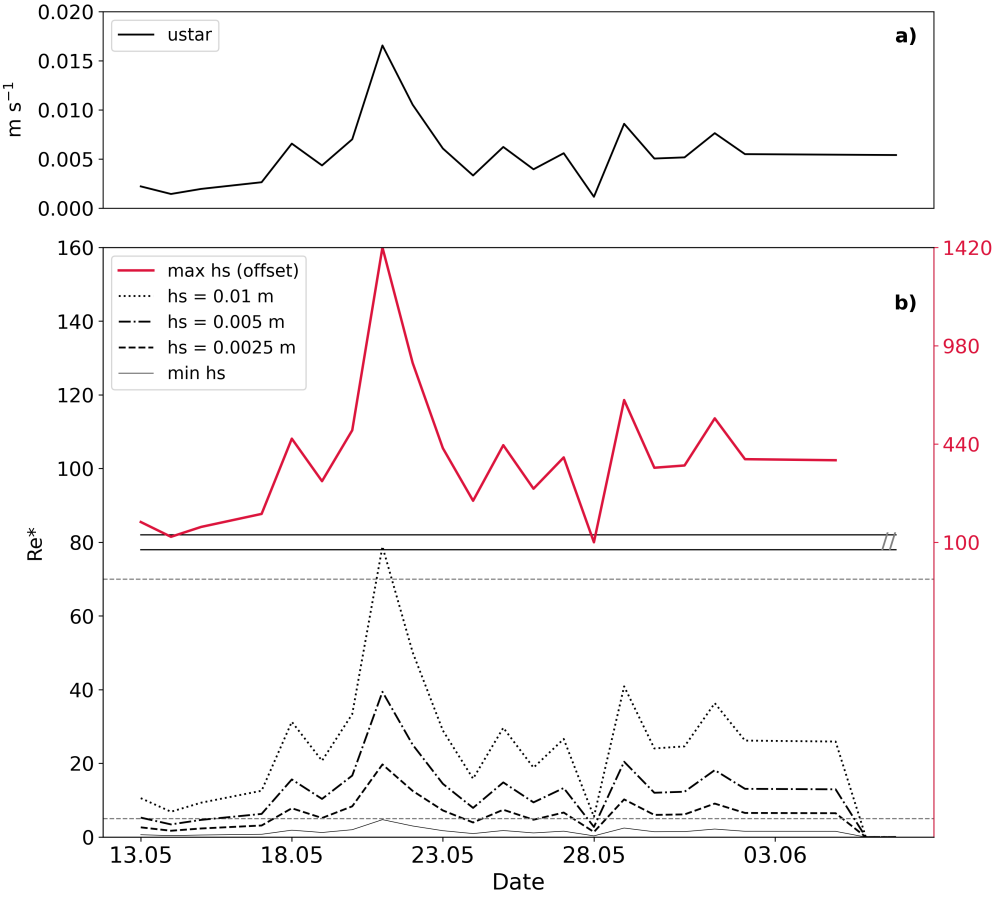

Figure 7. N-ICE2015 case study: a) Friction velocity; b) roughness Reynolds number Re* for the all the different size of roughness elements tested. The horizontal dashed lines at Re*= 5 and Re*= 70 depict the upper limit for a smooth flow and the lower limit for a rough turbulent flow, respectively. Note that the values of Re* for the maximum roughness (red colour) are represented on a different scale (y-axis on the right side).

https://doi.org/10.5194/egusphere-2025-5384
Preprint. Discussion started: 22 January 2026

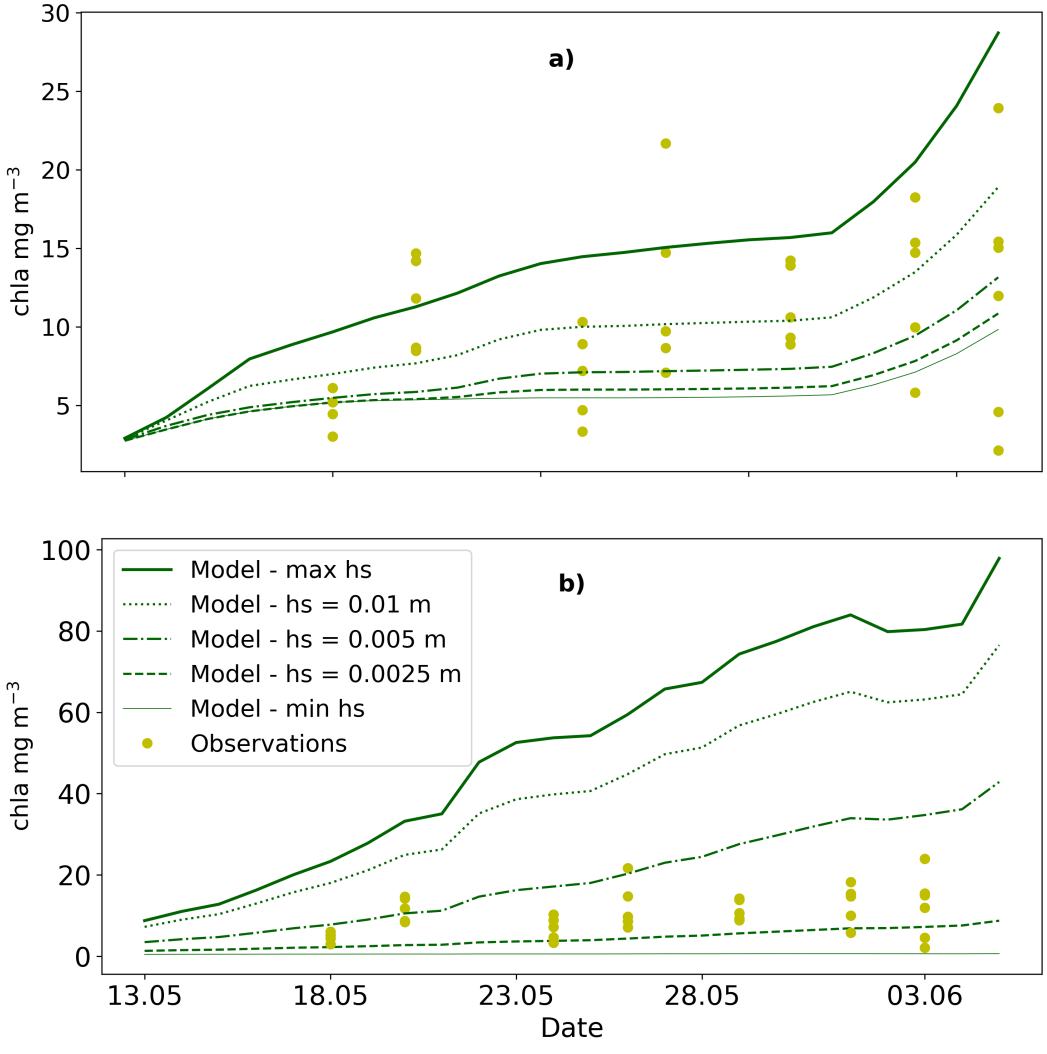

Figure 8. N-ICE2015 case study: Chl *a* concentrations at the sea ice bottom 10 cm in a) CICE + Icepack and b) SIMBAv2.0.

https://doi.org/10.5194/egusphere-2025-5384
Preprint. Discussion started: 22 January 2026

numbers ($Re^* < 40$). For the maximum roughness, the Reynolds number was still above the limit for turbulent flow (Figure 9b). For consistency with the depth range of the observations here we present average chl *a* concentrations for the bottom 3 cm (Figure 10). Observed values at the sea ice bottom were two orders of magnitude larger than those of the previous case studies. Both models predict chl *a* concentrations proportional to h_s but CICE + Icepack has an order of magnitude negative bias, even under the highest h_s, whereas SIMBAv2.0 may predict even larger values than the observed maximum. Irrespective of the h_s chosen, the CICE + Icepack model predicted strong nitrate depletion (Figure 11). At the start of the ice algal bloom, around mid-April, the depletion was confined to a narrow band just above the bottom layer, later on it expanded throughout the ice column (Figure 11).

4 Discussion

4.1 Parameterization of Ocean Fluxes

The physics governing the fluxes of nutrients at the ice-ocean interface happen at small scales that are not resolved by current sea ice models. The mixing and exchange processes thus need to be parameterized. Based on boundary layer and eddy-covariance studies, the flow at the ice-ocean interface that determines such exchanges can be smooth or turbulent, leading to molecular diffusion or turbulent driven exchanges, respectively (e.g., McPhee, 2008; Long et al., 2012). Many sea-ice biogeochemical models include one of these exchange types, with a preference for the former. However, the fluxes due to molecular diffusion (viscosity dominated) are often too small to provide enough nutrients to explain the biomass accumulation observed in the field (Dalman et al., 2019; Van der Linden et al., 2020; Roukaerts et al., 2021). This may be the reason why Lavoie et al. (2005) used a formulation based on molecular diffusion where the thickness of the boundary layer is calculated as a function of friction velocity, Jin et al. (2006) used a diffusion coefficient 4 orders of magnitude higher than the molecular diffusivity, and Watanabe et al. (2019) assumed that ice algae may uptake nutrients directly from seawater, based on a study by Boetius et al. (2013). However, this last study was focused on *Melosira arctica*, which forms aggregates or macroscopic strand colonies at the bottom-ice interface, whereas our focus is on the more common occurrence of ice algae living within the brine network and skeletal layer. Very few models parametrize the exchange fluxes as turbulent (e.g. Haddon et al., 2024), and none include the contribution of both viscosity and turbulence dominated regimes. In the present study we developed and implemented a new parameterization that accounts for the contribution of the two regimes allowing the flow to be in a transitional stage between smooth and turbulent. The fluxes are thus the result of a weighted contribution of both processes.

In our three case studies, we found that friction velocity was in the range of previous observations (McPhee, 2008, e.g.). Furthermore, we found that friction velocity was high enough to keep the flow in transition between smooth and turbulent. With low current velocity, and thus low friction velocity, viscous forces gain importance and the thickness of the molecular sublayer is such to limit the exchange fluxes. This was shown by (Long et al., 2012) during an eddy-covariance study in a southwest Greenland fjord, where stratification and low current velocities prevented the determination of oxygen fluxes during more than half of the instrument deployment time. Besides velocity, flow regime is determined also by under-ice roughness. It is indeed the ratio between the thickness of the molecular sublayer (function of u^*) and the height of the roughness elements h_s that

https://doi.org/10.5194/egusphere-2025-5384
Preprint. Discussion started: 22 January 2026

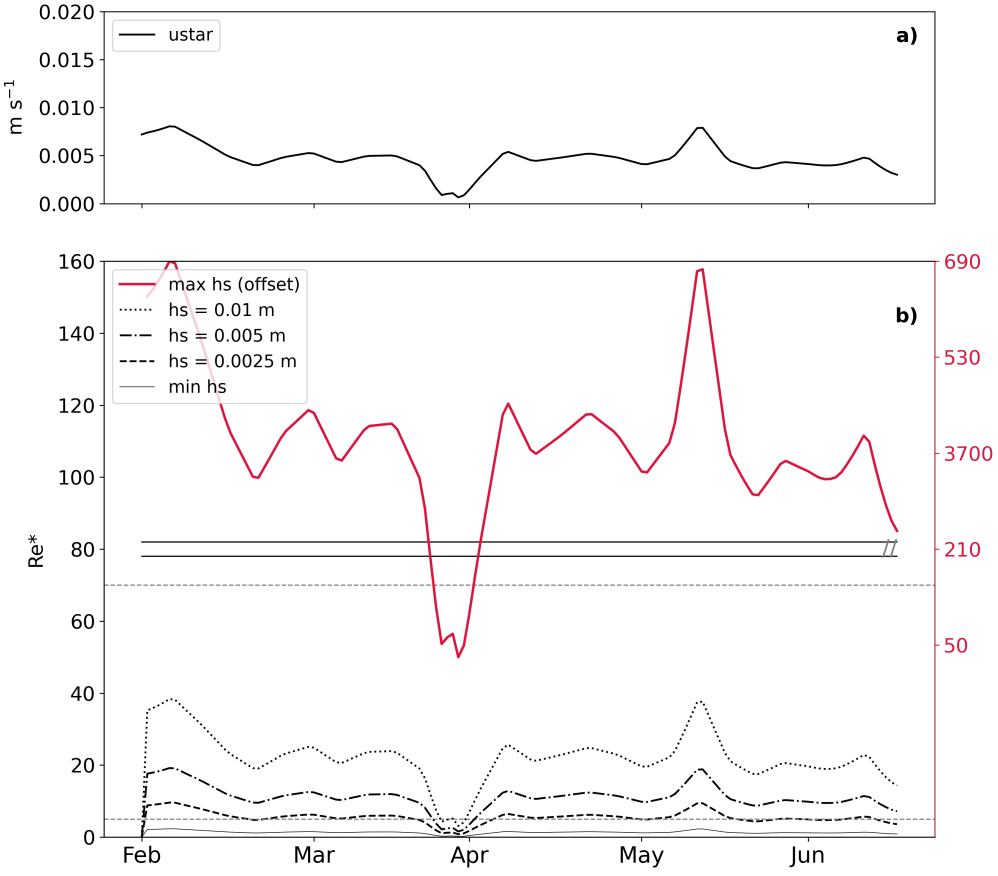

Figure 9. Resolute case study: a) Friction velocity; b) roughness Reynolds number Re^* for the all the different size of roughness elements tested. The horizontal dashed lines at Re^*= 5 and Re^*= 70 depict the upper limit for a smooth flow and the lower limit for a rough turbulent flow, respectively. Note that the values of Re^* for the maximum roughness (red colour) are represented on a different scale (y-axis on the right side).

https://doi.org/10.5194/egusphere-2025-5384
Preprint. Discussion started: 22 January 2026

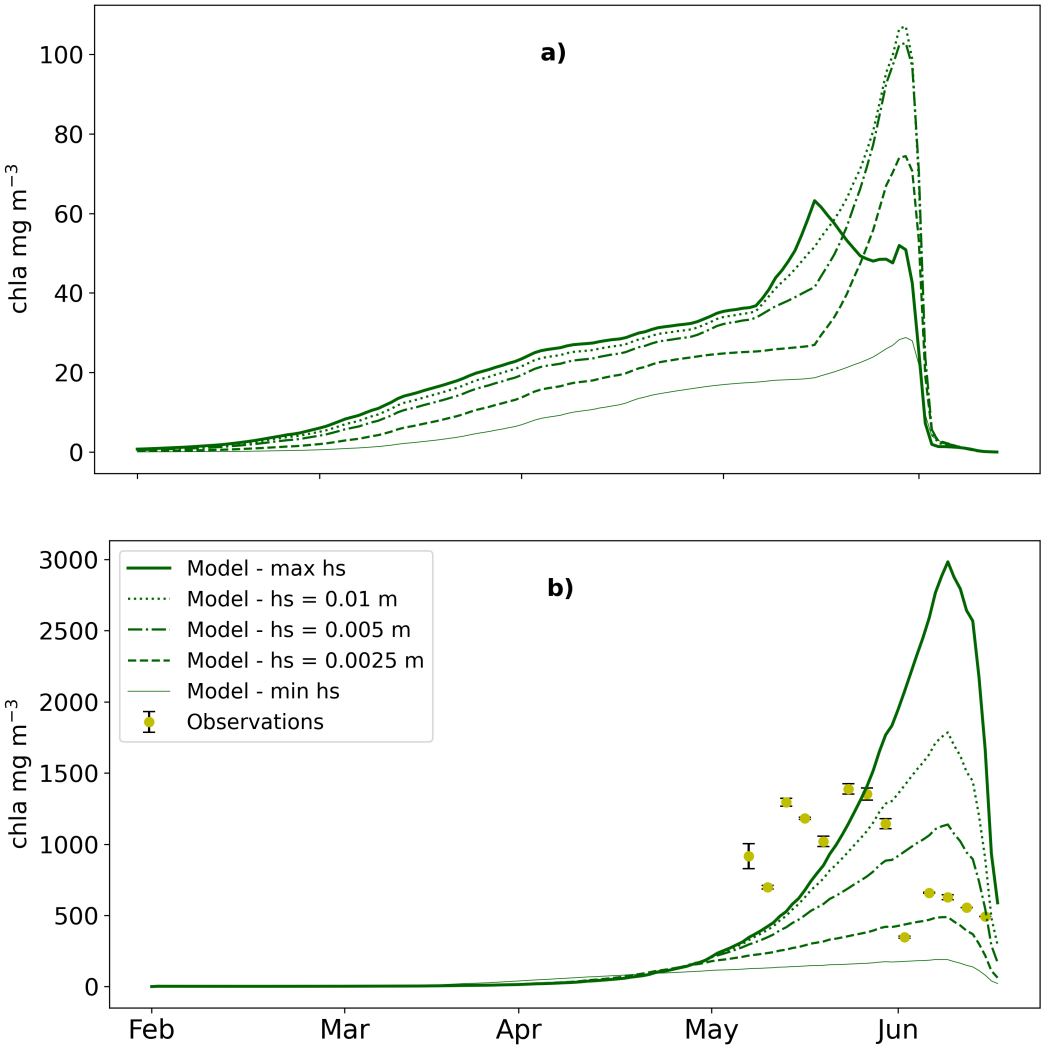

Figure 10. Resolute case study: Chl *a* concentrations at the sea ice bottom 3 cm in a) CICE + Icepack and b) SIMBAv2.0.

https://doi.org/10.5194/egusphere-2025-5384
Preprint. Discussion started: 22 January 2026

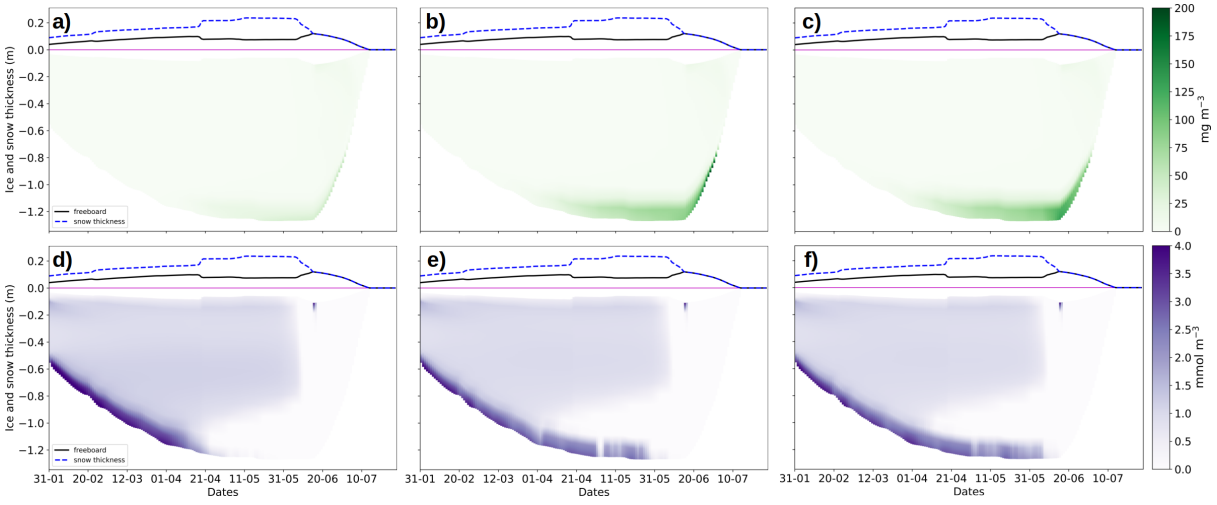

Figure 11. Resolute case study: Vertically resolved chl *a* and nitrate concentration (top row and lower rows, respectively) in CICE + Icepack in the case of a-d) minimum h_s; b-e) h_s = 0.005 m; c-f) maximum h_s. The blue dashed and the black lines represent snow height and freeboard, relative to the sea level (magenta line).

determines the nature of the flow (Nikuradse, 1933; Shirasawa and Ingram, 1991; Shirasawa and Grant Ingram, 1991; Kadivar et al., 2021); when roughness elements at the ice-ocean interface are larger than the thickness of the molecular sublayer the flow may shift from smooth to rough (see Supplementary material of Olsen et al., 2019, and references therein). This thickness of the molecular sublayer δz may be estimated with (Lavoie et al., 2005, and references therein):

$$\delta z = \frac{\nu}{u^*}. \tag{5}$$

For friction velocities in the range of the MOSAiC case study, the thickness of the molecular sublayer ranges between a maximum of 2 mm and a minimum of 0.1 mm. In Lavoie et al. (2005) the thickness of this sublayer was < 1 mm. The undersurface roughness in multiyear ice during the SHEBA experiment was 0.0048-0.007 m, i.e. around 6 mm (McPhee, 2002) and larger than our estimates of δz. We do not have information on the small scale roughness of the ice bottom in our three case studies, thus we tested different values covering the literature range. The range of variability of the thickness of the laminar sublayer and that of the surface roughness suggests that the flow under the sea ice may easily shift from smooth to turbulent, since the latter is larger than the former. The dependence on sea-ice roughness is a limitation of the current parameterization, since roughness measurements are usually not conducted during sea-ice monitoring. Moreover, it should be noted that the Reynolds number depends on the value of the oceanic drag coefficient through the friction velocity. We could have changed the value of the drag coefficient, which itself is a measure of surface roughness, rather than the roughness parameter directly. However, the drag coefficient in CICE + Icepack is also used in the momentum equation, thus we would have introduced other effects difficult to disentangle in our analysis.

https://doi.org/10.5194/egusphere-2025-5384
Preprint. Discussion started: 22 January 2026

In the MOSaiC case, our parameterization led to a simulated increase in ocean-to-ice nutrients fluxes that was proportional to roughness. The concentration of nutrients in the ice bottom did not vary substantially for most of the study, rather it rapidly equilibrated with the ocean concentration, but large changes occurred as soon as algal growth began, after release from light limitation. The two models showed different equilibrium concentrations, which were higher in SIMBAv2.0. This may be due to the fact that SIMBAv2.0 nutrients remain at the bottom ice, whereas in CICE + Icepack they diffuse vertically along the brine network, and thus the bottom brine concentration takes longer to equilibrate with the sea water and remains lower than in the former model. Both models, though, agree with observations (panel b in Figures 4 and 5), since the latter are scattered around 0.5 and 1.0 mmol m^{-3}, except for one large value at the end of March. This "outlier" may be attributed to a rafting event (Angelopoulos et al., 2022) and it is thus of dynamic nature (unresolved by our models). In July, observed values are lower and simulations with both models agree well, except for the maximum value of surface roughness in SIMBAv2.0. In both models, when only molecular diffusion is active, the ice bottom is rapidly depleted with nitrates after the bloom onset. This prevents any further algal growth.

4.2 Algal Phenology

In the MOSAiC case, modeled algal bloom started at the end of May. Algal growth led to an increase in nutrients fluxes, especially in CICE + Icepack case. This increase in nutrient fluxes does not lead to larger accumulation of nutrients in the ice bottom, but nutrients are rather utilized immediately by algae to sustain the growth. The higher the surface roughness parameter (thus, the higher the turbulence), the more algae can grow, and this holds for both models. The maximum biomass accumulated in the case of fully turbulent flux was almost four times larger than in the case of molecular diffusion. Initiation of growth, as well as timing of maximum biomass were not affected by the nature of the exchanges. Observations (Hoppe et al., 2024) show an initial increase in biomass at the beginning of April, which was not captured by either model. Between the beginning of May and mid July, no observations are available (Fong et al., 2024), thus it is not possible to know what was the maximum biomass accumulated during that time. The lack of growth in April in both models is due to the thick snow cover still present, on the order of 25 cm (e.g., Campbell et al., 2015, Figure 6). We note here that the forcing used to compute sea-ice thermodynamics and to compute light limitation for algae were collected with an IMB buoy located at distance from the FYI coring site (Lei et al., 2022). Unfortunately, none of the buoys located next to the coring site provided a time series long enough to simulate the ice growth during the entire drift period. As a result of this failure, as well as the inherent heterogeneity of the snow cover, the snow depths used to force the model may differ from those actually present at the FYI coring site. In both models algae start growing when snow melts and enough light is available to initiate the bloom. It should also be noted that this early growth in observations was unexpected (Hoppe et al., 2024) and probably due to very efficient light use from sea-ice algae, thus it is no surprise that models are not able to represent such early growth. Maximum biomass is reached at the same time for all different roughness values, but in SIMBAv2.0 the maximum occurs at the end of June, whereas in CICE + Icepack, it occurs at the beginning of July.

In the MOSAiC case, observations are sporadic so it is difficult to constrain model results. However, both in the N-ICE2015 and Resolute cases observations are available at higher time resolution. In the N-ICE2015 case, both models agreed with ob-

https://doi.org/10.5194/egusphere-2025-5384
Preprint. Discussion started: 22 January 2026

servations for at least 2-3 values of surface roughness considered. Both models simulated algal biomass accumulation, which was recorded in the refrozen lead. It has to be noted that CICE + Icepack was tuned (Duarte et al., 2017) to simulate the refrozen lead case before the parameterization was introduced, and when only molecular diffusion was considered (the default process in Icepack biogeochemistry). This explains why the case of minimum sea-ice roughness is able to capture the right accumulation of biomass. It should also be noted that the tuning carried out in Duarte et al. (2017) was independent of the flux parameterization. Specifically, Duarte et al. (2017) reduced the half-saturation constant for silicate uptake by 50%. While this adjustment affects ice-algal physiology and illustrates how tuning can be used to compensate for the absence of a more physically based representation of the system, such tuning may also reduce the model's realism by shifting physiological parameters away from observed or experimentally derived values. SIMBAv2.0 was not tuned on the N-ICE2015 data and the observed algal accumulation is properly simulated only when the contribution of turbulence is taken into account. However, SIMBAv2.0 utilizes parameters values as close as possible to those of CICE + Icepack, which may explain the better comparison with observations also for SIMBAv2.0 in the N-ICE2015 case. Resolute is a particular case characterized by very large biomass accumulation (Mortenson et al., 2017). Here, both models accumulated larger biomass compared to the other two cases, mainly due to the larger ocean nutrient concentrations than in the previous case studies. However, only SIMBAv2.0 was able to reproduce observations when the contribution of turbulence was taken into account, even though the maximum biomass was reached later (around June 7th) compared to observations. This shows the potential importance of turbulence in sustaining growth and in representing algal accumulation without relying on tuning parameters that are not well constrained by observations. The 1D model intercomparison of Tedesco et al. (Preprint) showed that the parameters that are often tuned to match observations are the half saturation constants and the chl *a* max specific growth rate. Although such tuning strategies allow better representation of observed phenology, they still fail in representing nutrients concentration in the ice. The model intercomparison of Tedesco et al. (Preprint) was focusing on Arctic data, however recently Lim et al. (2019) tuned the half saturation constant for silicate in an order to match a 17-day time series of biogeochemical sea-ice observations from Davis in East Antarctica. For CICE + Icepack, biomass values remained significantly lower compared to observations, even when the role of turbulence was included. One explanation could be that the redistribution of nutrients vertically does not happen fast enough for the bottom of the ice to be replenished by the amount of nutrients needed for algae to grow (Figure 11). Moreover, algae located higher in the ice have access to less nutrients and may grow slower, thus 'diluting' the overall growth. Finally, the vertical resolution of the model may not be appropriate to simulate the massive algal growth at its very bottom. In SIMBAv2.0 algae are forced to be located in the bottom 3 cm, whereas in CICE + Icepack the thickness of the bottom layer is the same as of the other layer of the biogrid and, possibly larger than 3 cm. Experiments not presented here showed that increasing vertical resolution (i.e. reducing the thickness of individual layers of the biogrid) leads to an overall increase in biomass concentration.

The response of the two models to the new parameterization was consistent: turbulence enhanced the nutrient fluxes at the ice-ocean interface. This led to a reduction in nutrient limitation and a significant increase in ice algal net primary production and chl a biomass accumulation in the ice, particularly in the bottom-ice. The parameterization performance was comparable in the two models presented in this study, so it may be used in models with different complexity. The fluxes have no influence on the onset of the bloom, which is determined by light availability, and also in this case the response of both models is consistent,

https://doi.org/10.5194/egusphere-2025-5384
Preprint. Discussion started: 22 January 2026

despite differences in calculating light limitation. In the MOSAiC case, ice algae started growing only after a decrease in snow depth since with thick snow light limitation is such to prevent any growth. This results points to two distinct limitation: on one hand the snow accumulation prescribed in the model and sued to force the physics may not be exactly representing the snow on top of the ice sampled with ice cores for biogeochemical analysis. On the other hand, algal physiology may be such that in reality algae can start growing at very low light levels (Hoppe et al., 2024) but the model is not able to represent such physiological trait. In general, SIMBAv2.0 accumulates more biomass than CICE + Icepack and it seems that the response of algae to enhanced nutrient fluxes is more sensitive. This appeared to be the case already with the previous version of SIMBA (Castellani et al., 2017) as it is shown in Tedesco et al., preprint. Despite the fact that SIMBAv2.0 is only a biogeochemical model, so it does not resolve physics, the main differences between the two models lie in the complexity of the biological processes. For example, CICE + Icepack includes ammonia; a temperature dependent description of mortality; a zooplankton term; a different parameterization of light limitation where light inhibition is also considered; and algal growth is also salinity and temperature dependent. On the other hand, SIMBAv2.0 presents a variable Chla:C ratio which results in a variable carbon to nitrogen ratio, whereas CICE + Icepack uses constant ratios. Finally, our results suggest that the vertical resolution plays an important role in the accumulation of biomass at the bottom of the ice.

5 Conclusions

We developed a parameterization that is well-grounded on the physics of the ocean-ice boundary layer, and accounts for the nature of the flow under sea ice, whether this is of smooth nature, of turbulent nature, or a combination of the two. The parameterization was implemented in two sea-ice biogeochemical models of different complexity to test its effects on the fluxes of nutrients at the ice-ocean interface. Our results show that when turbulence is taken into account, the fluxes of nutrients are much higher than those we could obtain with molecular diffusion alone. These enhanced fluxes can sustain larger accumulation of biomass for longer periods, consistently in both models. This seems to fill the "nutrient deficit" that pushed modellers to over-tune some physiological parameters in their models, or to accept that ice algae have direct access to ocean nutrients. We argue that turbulence should be considered when parameterizing nutrients exchanges, and that the implementation of the parameterization presented here can avoid the "cascading" changes that may incur when tuning a model, while at the same time adding realism to the simulations.

Code and data availability. The code for SIMBA can be downloaded at https://github.com/EyringMLClimateGroup/Castellani2025_GMD_SIMBA2 under DOI:10.5281/zenodo.17408325 (Castellani, 2025). CICE and Icepack are available, respectively, at https://github.com/pduarte8/CICE and https://github.com/pduarte8/Icepack under DOI:10.5281/zenodo.17383699 (Duarte, 2025a) and DOI:10.5281/zenodo.17394666 (Duarte, 2025b). Simulation results for both CICE + Icepack and SIMBA can be found at 10.21334/NPOLAR.2025.D8BD7FED.

https://doi.org/10.5194/egusphere-2025-5384
Preprint. Discussion started: 22 January 2026

Appendix A: SIMBAv2.0

The Sea Ice Model for Bottom algae (SIMBA) in its version 2.0 consists of three to five state variables describing the rate of change of ice algae, detritus and, one to three nutrients according to how many nutrients are used (nitrate, silicate, phosphate). The equation for sea-ice algae is:

$$\frac{\partial C_{\mathrm{Al}}}{\partial t} = \mu C_{\mathrm{Al}} - (\lambda_{\mathrm{Res}} + \lambda_{\mathrm{Mor}})\, C_{\mathrm{Al}}\,, \tag{A1}$$

where C_{Al} is the concentration of ice algae (mmol N m^{-3}) in the bottom of the ice δz. The thickness of the ice bottom can be set according to the resolution of the available observations. The second term on the right hand side of equation (A1) represent the algal loss due to mortality (λ_{Mor}) and respiration (λ_{Res}), both taken as constant with value of 0.01 d^{-1} for mortality and value of 0.005 d^{-1} for respiration. The first term represents the rate of algal growth due to primary production, which depends on nutrients and Photosynthetic Active Radiation (PAR) :

$$\mu = \mu_{\mathrm{M}} \min\left(L_{\mathrm{nit}}, L_{\mathrm{sil}}, L_{\mathrm{phos}}, L_{\mathrm{PAR}}\right), \tag{A2}$$

where μ_{M} represents the specific growth rate. The parameter μ_{M} is a tuning parameter and for the present study we use a value of 0.86 d^{-1} in the MOSAiC and Resolute case, and a value of 0.5 d^{-1} for the NICE case study (see discussion in Tedesco et al., Preprint). The nutrient limitation functions are based on the Monod formulation (Monod, 1949):

$$L_{\mathrm{N}} = \frac{C_N}{k_{\mathrm{N}} + C_N}\,, \tag{A3}$$

where C_N represents the concentrations of nitrate (mmol N m^{-3}), silicate (mmol Si m^{-3}) or phosphate (mmol P m^{-3}). k_{CN} is the half saturation constant for the nutrient chosen. Standard values in SIMBAv2.0 are k_{nit} = 1.6, k_{sil} = 3.9, and k_{phos} = 0.24 (Castellani et al., 2025). The light limitation function (L_{PAR}) is taken as in Jassby and Platt (1976):

$$L_{\mathrm{PAR}} = \tanh\left(\frac{\alpha \mathrm{PAR}}{P_{\mathrm{m}}}\right). \tag{A4}$$

In equation (A4) the photosynthetic efficiency α [gC (g Chl *a* hr μE m^{-2} s^{-1})] represents the increase of carbon assimilation per gram of chlorophyll for each unit increase in PAR. It indicates how quickly ice algae reach their light-saturated specific photosynthetic rate P_{m} [gC (g Chl *a* hr)$^{-1}$]. Various values are used in literature (see e.g., Lavoie et al., 2005), in the present study we use a value of α = 0.055. In SIMBAv2.0 we set only the value of α since we express P_{m} using Geider et al. (1998):

$$P_{\mathrm{m}} = \mu_{\mathrm{M}} \frac{L_{\mathrm{CN}}}{r_{\mathrm{C}}^{\mathrm{Chl}}}\,. \tag{A5}$$

https://doi.org/10.5194/egusphere-2025-5384
Preprint. Discussion started: 22 January 2026

We introduce in equation (A5) the Chl : C ratio $r_{\mathrm{C}}^{\mathrm{Chl}}$ (g g^{-1}) which we compute following Sibert et al. (2010):

$$r_{\mathrm{C}}^{\mathrm{Chl}} = r_{\mathrm{C}}^{\mathrm{Chl}}|_{\mathrm{max}} \left[0.25 + 0.75 \exp\left(-\frac{1}{2}\frac{\mathrm{PAR}}{k_{\mathrm{E}}}\right) L_{\mathrm{CN}}\right], \tag{A6}$$

where the half saturation parameter k_{E} is taken as 10 μE m^{-2} s^{-1}, and the maximum Chl : C ratio is taken as 0.1. The equations for the nutrients and for the detritus are given by:

$$\frac{\partial C_{\mathrm{nit}}}{\partial t} = -\left(\mu + \lambda_{\mathrm{Res}}\right) C_{\mathrm{Al}} + \lambda_{\mathrm{rm}} C_{\mathrm{Det}} + \beta, \tag{A7}$$

$$\frac{\partial C_{\mathrm{sil}}}{\partial t} = -R_{\mathrm{sn}} \left(\mu + \lambda_{\mathrm{Res}}\right) C_{\mathrm{Al}} + R_{\mathrm{sn}} \lambda_{\mathrm{rm}} C_{\mathrm{Det}} + \beta, \tag{A8}$$

$$\frac{\partial C_{\mathrm{phos}}}{\partial t} = -R_{\mathrm{pn}} \left(\mu + \lambda_{\mathrm{Res}}\right) C_{\mathrm{Al}} + R_{\mathrm{pn}} \lambda_{\mathrm{rm}} C_{\mathrm{Det}} + \beta, \tag{A9}$$

$$\frac{\partial C_{\mathrm{Det}}}{\partial t} = \lambda_{\mathrm{Mor}} C_{\mathrm{Al}} - \lambda_{\mathrm{rm}} C_{\mathrm{Det}}, \tag{A10}$$

where β is the source/sink of nutrients given by the parameterization described in Section 2.1. Silicate and phosphate are converted into nitrate units with the conversion factors R_{sn} = 1.8 for silicate to nitrate, and R_{pn} = 0.07 for phosphate to nitrate.

Author contributions. GC coded the model SIMBA2 and implemented the parameterizations in both models, conducted the simulations, analyzed the results, and drafted the manuscript. PD developed the study idea, contributed to implementing the parameterizations in CICE + Icepack and contributed to data analysis and manuscript drafting. KC and SB contributed to analysis of results and drafting of the manuscript.

Competing interests. The authors declare that no competing interests are present.

Acknowledgements. This study was supported by the BREATHE (Bottom sea ice Respiration and nutrient Exchanges Assessed for THE Arctic) project funded by the Research Council of Norway (grant no. 325405), by the European Union's Horizon 2020 research and innovation programme under grant no. 101003826 via project CRiceS, and the Norwegian Metacenter for Computational Science application NN10073K. GC also acknowledges funding by the Deutsche Forschungsgemeinschaft (DFG, German Research Foundation) through the Collaborative Research Centre TRR 181 "Energy Transfers in Atmosphere and Ocean" (project no. 274762653).

https://doi.org/10.5194/egusphere-2025-5384
Preprint. Discussion started: 22 January 2026

References

Angelopoulos, M., Damm, E., Simões Pereira, P., Abrahamsson, K., Bauch, D., Bowman, J., Castellani, G., Creamean, J., Divine, D. V., Dumitrascu, A., Fons, S. W., Granskog, M. A., Kolabutin, N., Krumpen, T., Marsay, C., Nicolaus, M., Oggier, M., Rinke, A., Sachs, T., Shimanchuk, E., Stefels, J., Stephens, M., Ulfsbo, A., Verdugo, J., Wang, L., Zhan, L., and Haas, C.: Deciphering the Properties of Different Arctic Ice Types During the Growth Phase of MOSAiC: Implications for Future Studies on Gas Pathways, Frontiers in Earth Science, Volume 10 - 2022, https://doi.org/10.3389/feart.2022.864523, 2022.

Arrigo, K. R., Kremer, J. N., and Sullivan, C. W.: A simulated Antarctic ast ice ecosystem, Journal of Geophysical Research: Oceans, 98, 6929–6946, https://doi.org/10.1029/93JC00141, 1993.

Arrigo, K. R., Worthen, D. L., Lizotte, M. P., Dixon, P., and Dieckmann, G.: Primary Production in Antarctic Sea Ice, Science, 276, 394–397, https://doi.org/10.1126/science.276.5311.394, 1997.

Ayata, S.-D., Lévy, M., Aumont, O., Sciandra, A., Sainte-Marie, J., Tagliabue, A., and Bernard, O.: Phytoplankton growth formulation in marine ecosystem models: Should we take into account photo-acclimation and variable stoichiometry in oligotrophic areas?, Journal of Marine Systems, 125, 29–40, https://doi.org/https://doi.org/10.1016/j.jmarsys.2012.12.010, advances in Marine Ecosystem Modelling Research III, 2013.

Boetius, A., Albrecht, S., Bakker, K., Bienhold, C., Felden, J., Fernández-Méndez, M., Hendricks, S., Katlein, C., Lalande, C., Krumpen, T., Nicolaus, M., Peeken, I., Rabe, B., R.-A., Rybakova, E., Somavilla, R., Wenzhöfer, F., and Sc, R. P. A.-.-S.: Export of Algal Biomass from the Melting Arctic Sea Ice, Science, 339, 1430–1432, https://doi.org/10.1126/science.1231346, 2013.

Campbell, K., Mundy, C., Barber, D., and Gosselin, M.: Characterizing the sea ice algae chlorophyll a–snow depth relationship over Arctic spring melt using transmitted irradiance, Journal of Marine Systems, 147, 76–84, https://doi.org/https://doi.org/10.1016/j.jmarsys.2014.01.008, the variability of primary production in the ocean: From the synoptic to the global scale. The 45th International Liege Colloquium on Ocean Dynamics, Liege, Belgium, May 13-17, 2013, 2015.

Castellani, G.: SIMBA2, https://doi.org/10.5281/zenodo.17408324, zenodo, DOI: 10.5281/zenodo.17408324, 2025.

Castellani, G., Losch, M., Lange, B. A., and Flores, H.: Modeling Arctic sea-ice algae: Physical drivers of spatial distribution and algae phenology, Journal of Geophysical Research: Oceans, 122, 7466–7487, https://doi.org/https://doi.org/10.1002/2017JC012828, 2017.

Castellani, G., Veyssière, G., Karcher, M., Stroeve, J.and Banas, S., Bouman, A., Brierley, S., Connan, S., Cottier, F., Große, F., Hobbs, L., Katlein, C., Light, B., McKee, D., Orkney, A., Proud, R., and Schourup-Kristensen, V.: Shine a light: Under-ice light and its ecological implications in a changing Arctic Ocean, Ambio, 51, 307–2017, https://doi.org/10.1007/s13280-021-01662-3, 2022.

Castellani, G., Tedesco, L., Steiner, N., and Vancoppenolle, M.: Numerical models of sea ice biogeochemistry, John Wiley & Sons, Ltd, 2025.

Cota, G. F. and Horne, E. P. W.: Physical Control of Arctic Ice Algal Production, Marine Ecology Progress Series, 52, 111–121, https://doi.org/10.3354/meps052111, 1989.

Cota, G. F. and Sullivan, C. W.: Photoadaptation, Growth and Production of Bottom Ice Algae in the Antarctic, Journal of Phycology, 26, 399–411, https://doi.org/10.1111/j.0022-3646.1990.00399.x, 1990.

Dalman, L. A., Else, B. G. T., Barber, D., Carmack, E., Williams, W. J., Campbell, K., Duke, P. J., Kirillov, S., and Mundy, C. J.: Enhanced bottom-ice algal biomass across a tidal strait in the Kitikmeot Sea of the Canadian Arctic, Elementa: Science of the Anthropocene, 7, 22, https://doi.org/10.1525/elementa.361, 2019.

https://doi.org/10.5194/egusphere-2025-5384
Preprint. Discussion started: 22 January 2026

Deal, C., Jin, M., Elliott, S., Hunke, E., Maltrud, M., and Jeffery, N.: Large-scale modeling of primary production and ice algal biomass within arctic sea ice in 1992, Journal of Geophysical Research: Oceans, 116, https://doi.org/10.1029/2010JC006409, c07004, 2011.

Duarte, P.: CICE release with MOSAiC and Resolute data types and h_iceruf, https://doi.org/10.5281/zenodo.4675096, zenodo, DOI: 10.5281/zenodo.4675096, 2025a.

Duarte, P.: Icepack release with MOSAiC and Resolute data types and h_iceruf, https://doi.org/10.5281/zenodo.4675020, zenodo, DOI: 10.5281/zenodo.4675020, 2025b.

Duarte, P., Meyer, A., Olsen, L. M., Kauko, H. M., Assmy, P., Rösel, A., Itkin, P., Hudson, S. R., Granskog, M. A., Gerland, S., Sundfjord, A., Steen, H., Hop, H., Cohen, L., Peterson, A. K., Jeffery, N., Elliott, S. M., Hunke, E. C., and Turner, A. K.: Sea ice thermohaline dynamics and biogeochemistry in the Arctic Ocean: Empirical and model results, Journal of Geophysical Research: Biogeosciences, 122, 1632–1654, https://doi.org/https://doi.org/10.1002/2016JG003660, 2017.

Duarte, P., Assmy, P., Campbell, K., and Sundfjord, A.: The importance of turbulent ocean–sea ice nutrient exchanges for simulation of ice algal biomass and production with CICE6.1 and Icepack 1.2, Geoscientific Model Development, 15, 841–857, https://doi.org/10.5194/gmd-15-841-2022, 2022.

Elliott, S., Deal, C., Humphries, G., Hunke, E., Jeffery, N., Jin, M., Levasseur, M., and Stefels, J.: Pan-Arctic simulation of coupled nutrient-sulfur cycling due to sea ice biology: Preliminary results, Journal of Geophysical Research: Biogeosciences, 117, https://doi.org/https://doi.org/10.1029/2011JG001649, 2012.

Fong, A. A., Hoppe, C. J. M., Aberle, N., Ashjian, C. J., Assmy, P., Bai, Y., Bakker, D. C. E., Balmonte, J. P., Barry, K. R., Bertilsson, S., Boulton, W., Bowman, J., Bozzato, D., Bratbak, G., Buck, M., Campbell, R. G., Castellani, G., Chamberlain, E. J., Chen, J., Chierici, M., Cornils, A., Creamean, J. M., Damm, E., Dethloff, K., Droste, E. S., Ebenhöh, O., Eggers, S. L., Engel, A., Flores, H., Fransson, A., Frickenhaus, S., Gardner, J., Gelfman, C. E., Granskog, M. A., Graeve, M., Havermans, C., Heuzé, C., Hildebrandt, N., Hill, T. C. J., Hoppema, M., Immerz, A., Jin, H., Koch, B. P., Kong, X., Kraberg, A., Lan, M., Lange, B. A., Larsen, A., Lebreton, B., Leu, E., Loose, B., Maslowski, W., Mavis, C., Metfies, K., Mock, T., Müller, O., Nicolaus, M., Niehoff, B., Nomura, D., Nöthig, E.-M., Oggier, M., Oldenburg, E., Olsen, L. M., Peeken, I., Perovich, D. K., Popa, O., Rabe, B., Ren, J., Rex, M., Rinke, A., Rokitta, S., Rost, B., Sakinan, S., Salganik, E., Schaafsma, F. L., Schäfer, H., Schmidt, K., Shoemaker, K. M., Shupe, M. D., Snoeijs-Leijonmalm, P., Stefels, J., Svenson, A., Tao, R., Torres-Valdés, S., Torstensson, A., Toseland, A., Ulfsbo, A., Van Leeuwe, M. A., Vortkamp, M., Webb, A. L., Zhuang, Y., and Gradinger, R. R.: Overview of the MOSAiC expedition: Ecosystem, Elementa: Science of the Anthropocene, 12, 00 135, https://doi.org/10.1525/elementa.2023.00135, 2024.

Geider, R. J., Maclntyre, H. L., and Kana, T. M.: A dynamic regulatory model of phytoplanktonic acclimation to light, nutrients, and temperature, Limnology and Oceanography, 43, 679–694, https://doi.org/https://doi.org/10.4319/lo.1998.43.4.0679, 1998.

Granskog, M. A., Fer, I., Rinke, A., and Steen, H.: Atmosphere-Ice-Ocean-Ecosystem Processes in a Thinner Arctic Sea Ice Regime: The Norwegian Young Sea ICE (N-ICE2015) Expedition, Journal of Geophysical Research-Oceans, 123, 1586–1594, https://doi.org/10.1002/2017jc013328, 2019.

Gu, F., Kauker, F., Yang, Q., Han, B., Fang, Y., and Liu, C.: Effects of Freezing Temperature Parameterization on Simulated Sea-Ice Thickness Validated by MOSAiC Observations, Geophysical Research Letters, 51, e2024GL108 281, https://doi.org/https://doi.org/10.1029/2024GL108281, e2024GL108281 2024GL108281, 2024.

Haddon, A., Farnole, P., Monahan, A. H., Sou, T., and Steiner, N.: Environmental controls and phenology of sea ice algal growth in a future Arctic, Elementa: Science of the Anthropocene, 12, 00 129, https://doi.org/10.1525/elementa.2023.00129, 2024.

https://doi.org/10.5194/egusphere-2025-5384
Preprint. Discussion started: 22 January 2026

Hayashida, H., Christian, J. R., Holdsworth, A. M., Hu, X., Monahan, A. H., Mortenson, E., Myers, P. G., Riche, O. G. J., Sou, T., and Steiner, N. S.: CSIB v1 (Canadian Sea-ice Biogeochemistry): a sea-ice biogeochemical model for the NEMO community ocean modelling framework, Geoscientific Model Development, 12, 1965–1990, https://doi.org/10.5194/gmd-12-1965-2019, 2019.

Hoppe, C., Fuchs, N., Notz, D., Anderson, P., Assmy, P., Berge, J., Bratbak, G., Guillou, G., Krabeg, A., Larsen, A., Lebreton, B., Leu, E., Lucassen, M., Müller, O., Oziel, L., Rost, B., Schartmüller, B., Torstensson, A., and Wloka, J.: Photosynthetic light requirement near the theoretical minimum detected in Arctic microalgae., Nat Commun, 15, https://doi.org/10.1038/s41467-024-51636-8, 2024.

Hunke, E. C., Lipscomb, W. H., Turner, A. K., Jeffery, N., and Elliott, S.: CICE: the Los Alamos Sea Ice Model Documentation and Software User's Manual Version 5.1, 2015.

Jassby, A. D. and Platt, T.: Mathematical formulation of the relationship between photosynthesis and light for phytoplankton, Limnology and Oceanography, 21, 540–547, https://doi.org/10.4319/lo.1976.21.4.0540, 1976.

Jeffery, N., Hunke, E. C., and Elliott, S. M.: Modeling the transport of passive tracers in sea ice, Journal of Geophysical Research: Oceans, 116, https://doi.org/https://doi.org/10.1029/2010JC006527, 2011.

Jeffery, N., Elliott, S. M., Hunke, E. C., Lipscomb, W. H., and Turner, A. K.: Biogeochemistry of CICE: the Los Alamos Sea Ice Model Documentation and Software User's Manual $zbgc_c olpkg$ modifications to Version 5, https://doi.org/10.2172/1329842, 2016.

Jin, M., Deal, J. C., Wang, J., Shin, K.-H., Tanaka, N., Whitledge, T. E., Lee, S. H., and Gradinger, R. R.: Controls of the landfast ice-ocean ecosystem offshore Barrow, Alaska, Annals of Glaciology, 44, 63–72, 2006.

Jin, M., Deal, C., Lee, S. H., Elliott, S., Hunke, E., Maltrud, M., and Jeffery, N.: Investigation of Arctic sea ice and ocean primary production for the period 1992–2007 using a 3-D global ice–ocean ecosystem model, Deep Sea Research II, 81, 2012.

Kadivar, M., Tormey, D., and McGranaghan, G.: A review on turbulent flow over rough surfaces: Fundamentals and theories, International Journal of Thermofluids, 10, 100 077, https://doi.org/https://doi.org/10.1016/j.ijft.2021.100077, 2021.

Lavoie, D., Denman, K., and Michel, C.: Modeling ice algal growth and decline in a seasonally ice-covered region of the Arctic (Resolute Passage, Canadian Archipelago), Journal of Geophysical Research: Oceans, 110, https://doi.org/10.1029/2005JC002922, c11009, 2005.

Lei, R., Cheng, B., Hoppmann, M., Zhang, F., Zuo, G., Hutchings, J. K., Lin, L., Lan, M., Wang, H., Regnery, J., Krumpen, T., Haapala, J., Rabe, B., Perovich, D. K., and Nicolaus, M.: Seasonality and timing of sea ice mass balance and heat fluxes in the Arctic transpolar drift during 2019–2020, Elementa: Science of the Anthropocene, 10, 000 089, https://doi.org/10.1525/elementa.2021.000089, 2022.

Leu, E., Mundy, C., Assmy, P., Campbell, K., Gabrielsen, T., Gosselin, M., Juul-Pedersen, T., and Gradinger, R.: Arctic spring awakening – Steering principles behind the phenology of vernal ice algal blooms, Progress in Oceanography, 139, 151–170, https://doi.org/10.1016/j.pocean.2015.07.012, overarching perspectives of contemporary and future ecosystems in the Arctic Ocean, 2015.

Light, B., Grenfell, T. C., and Perovich, D. K.: Transmission and absorption of solar radiation by Arctic sea ice during the melt season, Journal of Geophysical Research: Oceans, 113, https://doi.org/10.1029/2006JC003977, c03023, 2008.

Lim, S. M., Moreau, S., Vancoppenolle, M., Deman, F., Roukaerts, A., Meiners, K. M., Janssens, J., and Lannuzel, D.: Field Observations and Physical-Biogeochemical Modeling Suggest Low Silicon Affinity for Antarctic Fast Ice Diatoms, Journal of Geophysical Research: Oceans, 124, 7837–7853, https://doi.org/https://doi.org/10.1029/2018JC014458, 2019.

Long, M. H., Koopmans, D., Berg, P., Rysgaard, S., Glud, R. N., and Sogaard, D. H.: Oxygen exchange and ice melt measured at the ice-water interface by eddy correlation, Biogeosciences, 9, 1957–1967, https://doi.org/10.5194/bg-9-1957-2012, 2012.

Mann, K. and Lazier, J.: Biology and Boundary Layers, chap. 2, pp. 7–67, John Wiley & Sons, Ltd, ISBN 9781118687901, https://doi.org/https://doi.org/10.1002/9781118687901.ch2, 2005.

https://doi.org/10.5194/egusphere-2025-5384
Preprint. Discussion started: 22 January 2026

McPhee, M.: Turbulent heat and momentum transfer in the oceanic boundary layer under melting pack ice., J. Geophys. Res., 88(C5), 2827–2835, 1983.

McPhee, M.: Air-Ice-Ocean Interaction: Turbulent Ocean Boundary Layer Exchange Processes, Springer New York, New York, NY, ISBN 978-0-387-78335-2, https://doi.org/10.1007/978-0-387-78335-2_1, 2008.

McPhee, M. G.: The Effect of the Oceanic Boundary Layer on the Mean Drift of Pack Ice: Application of a Simple Model, Journal of Physical Oceanography, 9, 388 – 400, https://doi.org/10.1175/1520-0485(1979)009<0388:TEOTOB>2.0.CO;2, 1979.

McPhee, M. G.: Sea ice drag laws and simple boundary layer concepts, including application to rapid melting, Tech. rep., 1982.

McPhee, M. G.: Turbulent stress at the ice/ocean interface and bottom surface hydraulic roughness during the SHEBA drift, Journal of Geophysical Research-Oceans, 107, Artn 8037, https://doi.org/10.1029/2000jc000633, 2002.

Monod, J.: The Growth of Bacterial Cultures, Annual Review of Microbiology, 3, 371–394, https://doi.org/10.1146/annurev.mi.03.100149.002103, 1949.

Mortenson, E., Hayashida, H., Steiner, N., Monahan, A., Blais, M., Gale, M. A., Galindo, V., Gosselin, M., Hu, X., Lavoie, D., and Mundy, C. J.: A model-based analysis of physical and biological controls on ice algal and pelagic primary production in Resolute Passage, Elem Sci Anth., 50, https://doi.org/10.1525/elementa.229, 2017.

Mortenson, E., Steiner, N., Monahan, A. H., Miller, L. A., Geilfus, N.-X., and Brown, K.: A Model-Based Analysis of Physical and Biogeochemical Controls on Carbon Exchange in the Upper Water Column, Sea Ice, and Atmosphere in a Seasonally Ice-Covered Arctic Strait, Journal of Geophysical Research: Oceans, 123, 7529–7549, https://doi.org/https://doi.org/10.1029/2018JC014376, 2018.

Nicolaus, M., Katlein, C., Maslanik, J. A., and Hendricks, S.: Changes in Arctic sea ice result in increasing light transmittance and absorption, Geophys. Res. Lett., 39, 2699–2700, 2012.

Nicolaus, M., Perovich, D. K., Spreen, G., Granskog, M. A., von Albedyll, L., Angelopoulos, M., Anhaus, P., Arndt, S., Belter, H. J., Bessonov, V., Birnbaum, G., Brauchle, J., Calmer, R., Cardellach, E., Cheng, B., Clemens-Sewall, D., Dadic, R., Damm, E., de Boer, G., Demir, O., Dethloff, K., Divine, D. V., Fong, A. A., Fons, S., Frey, M. M., Fuchs, N., Gabarró, C., Gerland, S., Goessling, H. F., Gradinger, R., Haapala, J., Haas, C., Hamilton, J., Hannula, H.-R., Hendricks, S., Herber, A., Heuzé, C., Hoppmann, M., Høyland, K. V., Huntemann, M., Hutchings, J. K., Hwang, B., Itkin, P., Jacobi, H.-W., Jaggi, M., Jutila, A., Kaleschke, L., Katlein, C., Kolabutin, N., Krampe, D., Kristensen, S. S., Krumpen, T., Kurtz, N., Lampert, A., Lange, B. A., Lei, R., Light, B., Linhardt, F., Liston, G. E., Loose, B., Macfarlane, A. R., Mahmud, M., Matero, I. O., Maus, S., Morgenstern, A., Naderpour, R., Nandan, V., Niubom, A., Oggier, M., Oppelt, N., Pätzold, F., Perron, C., Petrovsky, T., Pirazzini, R., Polashenski, C., Rabe, B., Raphael, I. A., Regnery, J., Rex, M., Ricker, R., Riemann-Campe, K., Rinke, A., Rohde, J., Salganik, E., Scharien, R. K., Schiller, M., Schneebeli, M., Semmling, M., Shimanchuk, E., Shupe, M. D., Smith, M. M., Smolyanitsky, V., Sokolov, V., Stanton, T., Stroeve, J., Thielke, L., Timofeeva, A., Tonboe, R. T., Tavri, A., Tsamados, M., Wagner, D. N., Watkins, D., Webster, M., and Wendisch, M.: Overview of the MOSAiC expedition: Snow and sea ice, Elementa: Science of the Anthropocene, 10, 000 046, https://doi.org/10.1525/elementa.2021.000046, 2022.

Nikuradse, J.: Gesetzmäßigkeiten der turbulenten Strömung in glatten Rohren (Nachtrag), Forschung auf dem Gebiet des Ingenieurwesens A, 4, 44–44, 1933.

Nishi, Y. and Tabeta, S.: Analysis of the contribution of ice algae to the ice-covered ecosystem in Lake Saroma by means of a coupled ice–ocean ecosystem model, Journal of Marine Systems, 55, 249–270, https://doi.org/10.1016/j.jmarsys.2004.08.002, 2005.

Oggier, M., Salganik, E., Whitmore, L. M., Fong, A. A., Hoppe, C. J. M., Rember, R., Høyland, K. V., Gradinger, R., Divine, D. V., Fons, S. W., Abrahamsson, K., Aguilar-Islas, A. M., Angelopoulos, M., Arndt, S., Balmonte, J. P., Bozzato, D., Bowman, J. S., Castellani, G., Chamberlain, E., Creamean, J., D'Angelo, A., Damm, E., Dietrich, U., Droste, E. S., Dumitrascu, A., Eggers, L., Gardner, J., Grosfeld,

https://doi.org/10.5194/egusphere-2025-5384
Preprint. Discussion started: 22 January 2026

L., Haapala, J., Heitmann, L., Immerz, A., Kolabutin, N., Lange, B. A., Lei, R., Marsay, C. M., Maus, S., Müller, O., Olsen, L. M., Nuibom, A., Ren, J., Rinke, A., Schmidt, K., Sheikin, I., Shimanchuk, E., Snoeijs-Leijonmalm, P., Spahic, S., Stefels, J., Torres-Valdés, S., Torstensson, A., Ulfsbo, A., Verdugo, J., Vortkamp, M., Wang, L., Webster, M., and Granskog, M. A.: First-year sea-ice salinity, temperature, density, nutrient, oxygen and hydrogen isotope composition from the main coring site (MCS-FYI) during MOSAiC legs 1 to 4 in 2019/2020, version 2, https://doi.org/10.1594/PANGAEA.971385, 2024a.

Oggier, M., Salganik, E., Whitmore, L. M., Fong, A. A., Hoppe, C. J. M., Rember, R., Høyland, K. V., Gradinger, R., Divine, D. V., Fons, S. W., Abrahamsson, K., Aguilar-Islas, A. M., Angelopoulos, M., Arndt, S., Balmonte, J. P., Bozzato, D., Bowman, J. S., Castellani, G., Chamberlain, E., Creamean, J., D'Angelo, A., Damm, E., Dietrich, U., Droste, E. S., Dumitrascu, A., Eggers, S. L., Gardner, J., Grosfeld, L., Haapala, J., Heitmann, L., Immerz, A., Kolabutin, N., Lange, B. A., Lei, R., Marsay, C. M., Maus, S., Olsen, L. M., Müller, O., Nuibom, A., Ren, J., Rinke, A., Schmidt, K., Sheikin, I., Shimanchuk, E., Snoeijs-Leijonmalm, P., Spahic, S., Stefels, J., Torres-Valdés, S., Torstensson, A., Ulfsbo, A., Verdugo, J., Vortkamp, M., Wang, L., Webster, M., and Granskog, M. A.: Second-year sea-ice salinity, temperature, density, nutrient, oxygen and hydrogen isotope composition from the main coring site (MCS-SYI) during MOSAiC legs 1 to 4 in 2019/2020, https://doi.org/10.1594/PANGAEA.973860, 2024b.

Olsen, L. M., Duarte, P., Peralta-Ferriz, C., Kauko, H. M., Johansson, M., Peeken, I., Różańska-Pluta, M., Tatarek, A., Wiktor, J., Fernández-Méndez, M., Wagner, P. M., Pavlov, A. K., Hop, H., and Assmy, P.: A red tide in the pack ice of the Arctic Ocean, Scientific Reports, 9, 9536, https://doi.org/10.1038/s41598-019-45935-0, 2019.

Pogson, L., Tremblay, B., Lavoie, D., Michel, C., and Vancoppenolle, M.: Development and validation of a one-dimensional snow-ice algae model against observations in Resolute Passage, Canadian Arctic Archipelago, Journal of Geophysical Research: Oceans, 116, n/a–n/a, https://doi.org/10.1029/2010JC006119, c04010, 2011.

Rabe, B., Heuzé, C., Regnery, J., Aksenov, Y., Allerholt, J., Athanase, M., Bai, Y., Basque, C., Bauch, D., Baumann, T. M., Chen, D., Cole, S. T., Craw, L., Davies, A., Damm, E., Dethloff, K., Divine, D. V., Doglioni, F., Ebert, F., Fang, Y.-C., Fer, I., Fong, A. A., Gradinger, R., Granskog, M. A., Graupner, R., Haas, C., He, H., He, Y., Hoppmann, M., Janout, M., Kadko, D., Kanzow, T., Karam, S., Kawaguchi, Y., Koenig, Z., Kong, B., Krishfield, R. A., Krumpen, T., Kuhlmey, D., Kuznetsov, I., Lan, M., Laukert, G., Lei, R., Li, T., Torres-Valdés, S., Lin, L., Lin, L., Liu, H., Liu, N., Loose, B., Ma, X., McKay, R., Mallet, M., Mallett, R. D. C., Maslowski, W., Mertens, C., Mohrholz, V., Muilwijk, M., Nicolaus, M., O'Brien, J. K., Perovich, D., Ren, J., Rex, M., Ribeiro, N., Rinke, A., Schaffer, J., Schuffenhauer, I., Schulz, K., Shupe, M. D., Shaw, W., Sokolov, V., Sommerfeld, A., Spreen, G., Stanton, T., Stephens, M., Su, J., Sukhikh, N., Sundfjord, A., Thomisch, K., Tippenhauer, S., Toole, J. M., Vredenborg, M., Walter, M., Wang, H., Wang, L., Wang, Y., Wendisch, M., Zhao, J., Zhou, M., and Zhu, J.: Overview of the MOSAiC expedition: Physical oceanography, Elementa: Science of the Anthropocene, 10, 00 062, https://doi.org/10.1525/elementa.2021.00062, 2022.

Roukaerts, A., Deman, F., Van der Linden, F., Carnat, G., Bratkic, A., Moreau, S., Lannuzel, D., Dehairs, F., Delille, B., Tison, J.-L., and Fripiat, F.: The biogeochemical role of a microbial biofilm in sea ice: Antarctic landfast sea ice as a case study, Elementa: Science of the Anthropocene, 9, 00 134, https://doi.org/10.1525/elementa.2020.00134, 2021.

Shirasawa, K. and Grant Ingram, R.: Characteristics of the turbulent oceanic boundary layer under sea ice. Part 2: Measurements in southeast Hudson Bay, Journal of Marine Systems, 2, 161–169, https://doi.org/https://doi.org/10.1016/0924-7963(91)90022-M, 1991.

Shirasawa, K. and Ingram, R.: Characteristics of the turbulent oceanic boundary layer under sea ice. Part 1: A review of the ice-ocean boundary layer, Journal of Marine Systems, 2, 153–160, https://doi.org/https://doi.org/10.1016/0924-7963(91)90021-L, 1991.

Shupe, M. D., Rex, M., Blomquist, B., Persson, P. O. G., Schmale, J., Uttal, T., Althausen, D., Angot, H., Archer, S., Bariteau, L., Beck, I., Bilberry, J., Bucci, S., Buck, C., Boyer, M., Brasseur, Z., Brooks, I. M., Calmer, R., Cassano, J., Castro, V., Chu, D., Costa, D., Cox, C. J.,

https://doi.org/10.5194/egusphere-2025-5384
Preprint. Discussion started: 22 January 2026

Creamean, J., Crewell, S., Dahlke, S., Damm, E., de Boer, G., Deckelmann, H., Dethloff, K., Dütsch, M., Ebell, K., Ehrlich, A., Ellis, J., Engelmann, R., Fong, A. A., Frey, M. M., Gallagher, M. R., Ganzeveld, L., Gradinger, R., Graeser, J., Greenamyer, V., Griesche, H., Griffiths, S., Hamilton, J., Heinemann, G., Helmig, D., Herber, A., Heuzé, C., Hofer, J., Houchens, T., Howard, D., Inoue, J., Jacobi, H.-W., Jaiser, R., Jokinen, T., Jourdan, O., Jozef, G., King, W., Kirchgaessner, A., Klingebiel, M., Krassovski, M., Krumpen, T., Lampert, A., Landing, W., Laurila, T., Lawrence, D., Lonardi, M., Loose, B., Lüpkes, C., Maahn, M., Macke, A., Maslowski, W., Marsay, C., Maturilli, M., Mech, M., Morris, S., Moser, M., Nicolaus, M., Ortega, P., Osborn, J., Pätzold, F., Perovich, D. K., Petäjä, T., Pilz, C., Pirazzini, R., Posman, K., Powers, H., Pratt, K. A., Preußer, A., Quéléver, L., Radenz, M., Rabe, B., Rinke, A., Sachs, T., Schulz, A., Siebert, H., Silva, T., Solomon, A., Sommerfeld, A., Spreen, G., Stephens, M., Stohl, A., Svensson, G., Uin, J., Viegas, J., Voigt, C., von der Gathen, P., Wehner, B., Welker, J. M., Wendisch, M., Werner, M., Xie, Z., and Yue, F.: Overview of the MOSAiC expedition: Atmosphere, Elementa: Science of the Anthropocene, 10, 00 060, https://doi.org/10.1525/elementa.2021.00060, 2022.

Sibert, V., Zakardjian, B., Saucier, F., Gosselin, M., Starr, M., and Senneville, S.: Spatial and temporal variability of ice algal production in a 3D ice–ocean model of the Hudson Bay, Hudson Strait and Foxe Basin system, Polar Research, 29, 353–378, https://doi.org/10.1111/j.1751-8369.2010.00184.x, 2010.

Smith, R. E. H., Cavaletto, J. F., Eadie, B. J., and Gardner, W. S.: Growth and lipid composition of high Arctic ice algae during the spring bloom at Resolute, Northwest Territories, Canada, Mar. Ecol. Prog. Ser., 97, 19–29, 1993.

Smith, R. E. H., Gosselin, M., and Taguchi, S.: The influence of major inorganic nutrients on the growth and physiology of high Arctic ice algae, J. Mar. Syst., 110, 63–70, 1997.

Tedesco, L. and Vichi, M.: Sea Ice Biogeochemistry: A Guide for Modellers, PLoS ONE, 9, e89 217, http://www.ncbi.nlm.nih.gov/pmc/articles/PMC3934902, 2014.

Tedesco, L., Vichi, M., Haapala, J., and Stipa, T.: A dynamic Biologically Active Layer for numerical studies of the sea ice ecosystem, Ocean Modelling, 35, 89–104, https://doi.org/10.1016/j.ocemod.2010.06.008, 2010.

Tedesco, L., Steiner, N., and Peeken, I.: Sea-ice ecosystems, in: Reference Module in Earth Systems and Environmental Sciences, Elsevier, ISBN 978-0-12-409548-9, https://doi.org/https://doi.org/10.1016/B978-0-323-85242-5.00043-9, 2025.

Tedesco, L., Castellani, G.and Duarte, P., Jin, M., Moreau, S., Mortenson, E., Saenz, B., Steiner, N., and Vancoppenolle, M.: Insights into sea-ice biogeochemistry: An intercomparison of process models, nd, nd, nd, https://doi.org/nd, Preprint.

Torres-Valdés, S., Rember, R., Heitmann, L., Ludwichowski, K.-U., Ulfsbo, A., Fong, A. A., Hoppe, C. J. M., Kuznetsov, I., Damm, E., Graeve, M., Dietrich, U., Chamberlain, E., Droste, E. S., Creamean, J., Gardner, J., Müller, O., Balmonte, J. P., and Rost, B.: Dissolved nutrients data from the PS122 MOSAiC Expedition carried out onboard Polarstern during Legs 1 to 3, https://doi.org/10.1594/PANGAEA.966213, 2024a.

Torres-Valdés, S., Rember, R., Heitmann, L., Ludwichowski, K.-U., Ulfsbo, A., Fong, A. A., Hoppe, C. J. M., Kuznetsov, I., Damm, E., Graeve, M., Dietrich, U., Chamberlain, E., Droste, E. S., Creamean, J., Gardner, J., Müller, O., Balmonte, J. P., and Rost, B.: Dissolved nutrients data from the PS122 MOSAiC Expedition carried out at the AWI Nutrient Facility, https://doi.org/10.1594/PANGAEA.966217, 2024b.

Van der Linden, F. C., Tison, J.-L., Champenois, W., Moreau, S., Carnat, G., Kotovitch, M., Fripiat, F., Deman, F., Roukaerts, A., Dehairs, F., Wauthy, S., Lourenço, A., Vivier, F., Haskell, T., and Delille, B.: Sea Ice CO2 Dynamics Across Seasons: Impact of Processes at the Interfaces, Journal of Geophysical Research: Oceans, 125, e2019JC015 807, https://doi.org/https://doi.org/10.1029/2019JC015807, e2019JC015807 2019JC015807, 2020.

https://doi.org/10.5194/egusphere-2025-5384
Preprint. Discussion started: 22 January 2026

Vancoppenolle, M., Goosse, H., de Montety, A., Fichefet, T., Tremblay, B., and Tison, J.-L.: Modeling brine and nutrient dynamics in Antarctic sea ice: The case of dissolved silica, Journal of Geophysical Research: Oceans, 115, https://doi.org/https://doi.org/10.1029/2009JC005369, 2010.

Watanabe, E., Onodera, J., Harada, N., Aita, M. N., Ishida, A., and Kishi, M. J.: Wind-driven interannual variability of sea ice algal production in the western Arctic Chukchi Borderland, Biogeosciences, 12, 6147–6168, https://doi.org/10.5194/bg-12-6147-2015, 2015.

Watanabe, E., Jin, M., Hayashida, H., Zhang, J., and Steiner, N.: Multi-Model Intercomparison of the Pan-Arctic Ice-Algal Productivity on Seasonal, Interannual, and Decadal Timescales, Journal of Geophysical Research: Oceans, 124, 9053–9084, https://doi.org/https://doi.org/10.1029/2019JC015100, 2019.